



Final Targeting Strategy for the SDSS-IV APOGEE-2S Survey

Felipe A. Santana¹, Rachael L. Beaton^{2,3,39,40}, Kevin R. Covey⁴, Julia E. O’Connell⁵, Penélope Longa-Peña⁶, Roger Cohen⁷, José G. Fernández-Trincado^{8,9}, Christian R. Hayes¹⁰, Gail Zasowski¹¹, Jennifer S. Sobek¹⁰, Steven R. Majewski¹², S. D. Chojnowski^{13,14}, Nathan De Lee^{15,16}, Ryan J. Oelkers¹⁶, Guy S. Stringfellow¹⁷, Andrés Almeida¹², Borja Anguiano^{12,19}, John Donor²⁰, Peter M. Frinchaboy²⁰, Sten Hasselquist^{11,41}, Jennifer A. Johnson²¹, Juna A. Kollmeier³, David L. Nidever¹⁴, Adrian M. Price-Whelan²², Alvaro Rojas-Arriagada^{23,24}, Mathias Schultheis²⁵, Matthew Shetrone²⁶, Joshua D. Simon³, Conny Aerts²⁷, Jura Borissova^{24,28}, Maria R. Drout^{3,29}, Doug Geisler^{5,18,30}, C. Y. Law^{31,32}, Nicolas Medina^{24,28}, Dante Minniti^{33,34}, Antonela Monachesi^{18,30}, Ricardo R. Muñoz¹, Radosław Poleski^{21,35}, Alexandre Roman-Lopes³⁰, Kevin C. Schlafman³⁶, Amelia M. Stutz⁵, Johanna Teske^{37,42}, Andrew Tkachenko²⁷, Jennifer L. Van Saders³⁸, Alycia J. Weinberger³⁷, and Manuela Zoccali^{23,24}

¹ Departamento de Astronomía, Universidad de Chile, Camino El Observatorio 1515, Las Condes, Santiago, Chile; fsantana@das.uchile.cl

² Department of Astrophysical Sciences, Princeton University, 4 Ivy Lane, Princeton, NJ 08544, USA

³ The Observatories of the Carnegie Institution for Science, 813 Santa Barbara Street, Pasadena, CA 91101, USA

⁴ Department of Physics & Astronomy, Western Washington University, Bellingham, WA 98225, USA

⁵ Departamento de Astronomía, Universidad de Concepción, Casilla 160-C, Concepción, Chile

⁶ Centro de Astronomía, Universidad de Antofagasta, Avenida Angamos 601, Antofagasta 1270300, Chile

⁷ Space Telescope Science Institute, Baltimore, MD 21218, USA

⁸ Instituto de Astronomía, Universidad Católica del Norte, Av. Angamos 0610, Antofagasta, Chile

⁹ Universidad de Atacama, Copayapu 485, Copiapó, Chile

¹⁰ Department of Astronomy, University of Washington, Seattle, WA 98195, USA

¹¹ Department of Physics & Astronomy, University of Utah, Salt Lake City, UT 84112, USA

¹² Department of Astronomy, University of Virginia, Charlottesville, VA 22903, USA

¹³ Department of Astronomy, New Mexico State University, Las Cruces, NM 88001, USA

¹⁴ Department of Physics, Montana State University, P.O. Box 173840, Bozeman, MT 59717-3840, USA

¹⁵ Department of Physics, Geology, and Engineering Technology, Northern Kentucky University, Highland Heights, KY 41099, USA

¹⁶ Department of Physics & Astronomy, Vanderbilt University, Nashville, TN 37235, USA

¹⁷ Center for Astrophysics and Space Astronomy, Department of Astrophysical and Planetary Sciences, University of Colorado, Boulder, CO 80309, USA

¹⁸ Instituto de Investigación Multidisciplinario en Ciencia y Tecnología, Universidad de La Serena, Avenida Raúl Bitrán S/N, La Serena, Chile

¹⁹ Department of Physics & Astronomy, Macquarie University, Balaclava Rd, NSW 2109, Australia

²⁰ Department of Physics & Astronomy, Texas Christian University, Fort Worth, TX 76129, USA

²¹ Department of Astronomy, The Ohio State University, Columbus, OH 43210, USA

²² Center for Computational Astrophysics, Flatiron Institute, 162 Fifth Ave, New York, NY 10010, USA

²³ Instituto de Astrofísica, Facultad de Física, Pontificia Universidad Católica de Chile, Av. Vicuña Mackenna 4860, Santiago, Chile

²⁴ Millennium Institute of Astrophysics, Av. Vicuña Mackenna 4860, 782-0436, Macul, Santiago, Chile

²⁵ Observatoire de la Côte d’Azur, Lagrange Boulevard de l’Observatoire, F-06304 Nice, France

²⁶ University of California Observatories, Santa Cruz, CA 95064, USA

²⁷ Institute of Astronomy, KU Leuven, Celestijnenlaan 200D, B-3001 Leuven, Belgium

²⁸ Instituto de Física y Astronomía, Universidad de Valparaíso, Av. Gran Bretaña 1111, Playa Ancha, Casilla 5030, Chile

²⁹ Department of Astronomy and Astrophysics, University of Toronto, 50 St. George St, Toronto, Ontario, M5S 3H4 Canada

³⁰ Departamento de Astronomía, Facultad de Ciencias, Universidad de La Serena. Av. Juan Cisternas 1200, La Serena, Chile

³¹ Department of Space, Earth & Environment, Chalmers University of Technology, SE-412 96 Gothenburg, Sweden

³² Department of Physics, The Chinese University of Hong Kong, Shatin, NT, SAR, Hong Kong

³³ Departamento de Ciencias Físicas, Facultad de Ciencias Exactas, Universidad Andrés Bello, Fernández Concha 700, Las Condes, Santiago, Chile

³⁴ Vatican Observatory, Vatican City State, V-00120, Italy

³⁵ Astronomical Observatory, University of Warsaw, Al. Ujazdowskie 4, 00-478 Warszawa, Poland

³⁶ Department of Physics and Astronomy, Johns Hopkins University, 3400 N Charles Street, Baltimore, MD 21218, USA

³⁷ Earth and Planets Laboratory, Carnegie Institution for Science, 5241 Broad Branch Road, NW, Washington, DC 20015, USA

³⁸ Institute for Astronomy, University of Hawai’i, 2680 Woodlawn Drive, Honolulu, HI 96822, USA

Received 2020 December 7; revised 2021 September 24; accepted 2021 October 3; published 2021 December 9

Abstract

APOGEE is a high-resolution ($R \sim 22,000$), near-infrared, multi-epoch, spectroscopic survey of the Milky Way. The second generation of the APOGEE project, APOGEE-2, includes an expansion of the survey to the Southern Hemisphere called APOGEE-2S. This expansion enabled APOGEE to perform a fully panoramic mapping of all of the main regions of the Milky Way; in particular, by operating in the H band, APOGEE is uniquely able to probe the dust-hidden inner regions of the Milky Way that are best accessed from the Southern Hemisphere. In this paper we present the targeting strategy of APOGEE-2S, with special attention to documenting modifications to the original, previously published plan. The motivation for these changes is explained as well as an assessment of their

³⁹ Much of this work was completed while this author was a NASA Hubble Fellow at Princeton University.

⁴⁰ Carnegie-Princeton Fellow.

⁴¹ NSF Astronomy and Astrophysics Postdoctoral Fellow.

⁴² Much of this work was completed while this author was a NASA Hubble Fellow at the Observatories of the Carnegie Institution for Science.

effectiveness in achieving their intended scientific objective. In anticipation of this being the last paper detailing APOGEE targeting, we present an accounting of all such information complete through the end of the APOGEE-2S project; this includes several main survey programs dedicated to exploration of major stellar populations and regions of the Milky Way, as well as a full list of programs contributing to the APOGEE database through allocations of observing time by the Chilean National Time Allocation Committee and the Carnegie Institution for Science. This work was presented along with a companion article, Beaton et al. (2021), presenting the final target selection strategy adopted for APOGEE-2 in the Northern Hemisphere.

Unified Astronomy Thesaurus concepts: [Galaxy dynamics \(591\)](#); [Galaxy kinematics \(602\)](#); [Galaxy formation \(595\)](#); [Galaxy evolution \(594\)](#); [Galaxy abundances \(574\)](#); [Galaxy structure \(622\)](#); [Galaxy stellar content \(621\)](#); [Milky Way Galaxy \(1054\)](#); [Astronomy databases \(83\)](#); [Surveys \(1671\)](#)

1. Introduction

The Apache Point Galactic Evolution Experiment (APOGEE; Majewski et al. 2017)⁴³ is a high-resolution ($R \sim 22,500$), near-infrared (NIR; $\lambda = 1.51\text{--}1.70 \mu\text{m}$), multi-epoch, spectroscopic survey of the Milky Way. During its first generation (2011–2014; hereafter APOGEE-1), the survey was one of the projects within the Sloan Digital Sky Survey (SDSS) III (Eisenstein et al. 2011), and provided spectra for $\sim 163,000$ stars with a signal-to-noise ratio (S/N) of ~ 100 , covering a large variety of Galactic environments. Along with the spectra, APOGEE-1 provided high level data products derived from the spectra—fundamental stellar parameters like radial velocity, effective temperature, surface gravity, and chemical abundances for 15 elements, the latter derived via the APOGEE Stellar Parameter and Chemical Abundance Pipeline (ASPCAP; García Pérez et al. 2016); the cumulative results from APOGEE-1 were released in DR12 (Holtzman et al. 2015).

APOGEE data have been applied to a wide variety of topics in stellar astrophysics and Galactic archeology. APOGEE-enabled research covers a wide range of Galactic environments allowing for the detailed study of the Milky Way’s main structures: the disk (most recently, Mackereth et al. 2019a; Hasselquist et al. 2019a; Eilers et al. 2019; Frankel et al. 2019; Donor et al. 2020), the bulge (most recently, Hasselquist et al. 2020; Rojas-Arriagada et al. 2020; Griffith et al. 2021), and the halo (most recently, Mackereth et al. 2019b; Fernández-Alvar et al. 2019; Mackereth & Bovy 2020), as well as its constituent globular clusters, satellite galaxies, and tidal streams (most recently, Hasselquist et al. 2019b; Masseron et al. 2019; Hayes et al. 2020; Horta et al. 2020; Mészáros et al. 2020).

In addition to better understanding the Milky Way through classic Galactic astronomy exploration, as APOGEE-1 was originally designed to perform, the APOGEE data set has also been used to study scientific fields outside of its original intent, delving into stellar astrophysics (most recently, Pinsonneault et al. 2018; Mackereth et al. 2021), studies of the interstellar medium (ISM; Schultheis et al. 2014; Zasowski et al. 2015b, 2015a), and even time series analyses of radial velocity variability as an indicator of stellar companions (most recently, Clark Cunningham et al. 2019; Price-Whelan et al. 2020; Mazzola et al. 2020), planet hosts (most recently, Cañas et al. 2019a, 2019b), and intrinsically variable stars (most recently, Chojnowski et al. 2019, 2020; Lewis et al. 2020).

This diversity of topics addressed is only possible because of the efforts put into the careful creation of the APOGEE data,

which, on the one hand, needs to sample a broad range of stellar types and populations, but, on the other hand, must be chosen with simple enough criteria that a reliable selection function can be generated. The selection criteria used to select stars for the different science programs in APOGEE-1 were presented in Zasowski et al. (2013), which includes details on how these criteria have been optimized for the survey science goals, the tools required to calculate and account for the selection function, and how the different selection methods are identified using a set of targeting bits.

The second generation of the APOGEE project (APOGEE-2; S. Majewski et al. 2021, in preparation) is part of SDSS-IV (2014–2020; Blanton et al. 2017), and uses near-twin spectrographs (described in Wilson et al. 2019) operating simultaneously in the Northern and Southern Hemispheres. The APOGEE-N spectrograph, the original spectrograph used for APOGEE-1, remains mounted on the Sloan Foundation 2.5 m telescope at the Apache Point Observatory (APO; Gunn et al. 2006), and is carrying out observations for the APOGEE-2 North (APOGEE-2N) program, while a second, near-clone spectrograph, APOGEE-S, (Wilson et al. 2019) is mounted on the Irénée du Pont 2.5 m telescope (Bowen & Vaughan 1973) at Las Campanas Observatory (LCO), where it is used to execute the APOGEE-2 South (APOGEE-2S) observing program.

The expansion to the Southern Hemisphere in APOGEE-2 has provided the survey a truly panoramic view of the Milky Way, but, particularly, its “dust-hidden” inner regions. The initial observational design of APOGEE-2 was explained in Zasowski et al. (2017, hereafter Z17), which included a detailed description for each of the distinct science programs planned for APOGEE-2 and was published alongside the first data release from APOGEE-2 (in DR14; Abolfathi et al. 2018; Holtzman et al. 2018), which contained only data from APOGEE-N. We note that the Z17 survey plan for APOGEE-2S was schematic in nature, as the APOGEE-S instrument was still being commissioned at the time of writing. It also included a general overview of a survey component unique to APOGEE-2S, that of Contributed Programs, observations allocated outside of SDSS-IV via proposals to use the APOGEE-S instrument through either the Chilean National Time Allocation Committee (CNTAC) or the Time Allocation Committee (TAC) for the Observatories of the Carnegie Institution for Science (OCIS). However, Z17 was written before survey observations on the du Pont had commenced, and before the first Contributed Programs had even been scheduled⁴⁴. Thus, the first description of APOGEE-2S targeting (Z17) both did not contain details for the Contributed Programs

⁴³ The nomenclature we will use is as follows: APOGEE refers to the joint APOGEE-1 and APOGEE-2 project or tools common to it, APOGEE-N or APOGEE-S refer to the spectrographs in the Northern and Southern Hemisphere, respectively, and APOGEE-1 or APOGEE-2 refer to the SDSS-III and SDSS-IV surveys, respectively.

⁴⁴ Time for Contributed Programs was allocated for observing semesters starting in 2017A and continued until 2020A.

and assumed that APOGEE-1 or APOGEE-2N strategies would largely be adopted identically for APOGEE-2S.

The main goal of this paper is to present the targeting strategy adopted for APOGEE-2S through the final stage of the APOGEE-2S operations that ended in 2021 January. The target selection methods for APOGEE-2S have evolved since the publication of Z17, and hence, could not have been contained in that or other past references. Such changes were implemented after a detailed consideration of the early on-sky performance from APOGEE-2S (DR16 was the first public release of data obtained with APOGEE-S spectrograph; Ahumada et al. 2020; Jönsson et al. 2020), in particular, the true observing efficiency and instrumental throughput. With the experience and operational strategies of APOGEE-1 and APOGEE-2N in hand (see the concluding section of R. Beaton et al., submitted; AAS29028), we were able to optimize the observations for APOGEE-2S in a timely manner. We demonstrate how those modifications not only increase the likelihood of reaching our initial scientific goals, but also enable us to exceed them in many cases.

Alongside this present paper, R. Beaton et al. (submitted; AAS29028) presents the final targeting strategy of APOGEE-2N, which is focused on its Bright Time eXtension and ancillary programs. Both papers are intended to complete the references about APOGEE target selection and complement the existing APOGEE targeting selection references (Z13, Z17), the data release references (Ahumada et al. 2020; Jönsson et al. 2020), and our online documentation (e.g., <https://www.sdss.org/dr16/> for DR16, <https://www.sdss.org/dr17/> for DR17). Together, these papers present the final field plan spatial coverage of APOGEE-2, as well as the statistics of our observing schedule. The papers focus on how the targeting strategy changed from that presented in Z17, explaining these differences for each scientific program separately, and also detailing the characteristics of any new programs. These articles also represent a unique opportunity to analyze how the differences between APOGEE-2S and APOGEE-2N, in terms of time line of implementation, observing time availability per local sidereal time (LST), and telescope characteristics, impacted the targeting strategy and observing progress for some programs. In this paper dedicated to APOGEE-2S we also present descriptions for each of the programs contributed to the SDSS-IV survey from CIS and CNTAC allocations; the Contributed Programs represent $\sim 23\%$ of the total observing time for APOGEE-2S survey from 2017 to 2020 (for comparison, the APOGEE-2N Ancillary Programs were approximately 5% of the six-year program) and are a significant component of the APOGEE-2s data set.

The outline of the paper is as follows. Section 2 defines key concepts associated with SDSS-IV and APOGEE that are relevant to targeting. Section 3 gives an overview of how the different types of APOGEE-2S fibers (science, sky, and calibration) are assigned. Changes to the original field plan and targeting strategy for APOGEE-2S are given in Section 4 and this section includes a table that summarizes the main scientific programs. Contributed Programs are detailed in Section 5. A summary is given in Section 6. A glossary of common terms used in this paper is presented in the Appendix to aid the reader.

2. APOGEE Observations and Targeting Basics

In this section, we provide a summary of the primary methods used for selecting targets in APOGEE; much of this

material is also presented in Z13, Z17, and R. Beaton et al. (submitted; AAS29028), because these are the core set of principles guiding the design of all APOGEE observations. Key SDSS- and APOGEE-specific concepts and terms affiliated with the process are described and defined; such terms are first introduced in quotation marks (e.g., “term”) to indicate that they are specific technical terms. The key nomenclature are also organized as a Glossary in the Appendix as a convenience (following that of Z13 and Z17, but also including the new terms used for this present paper). We also note that this section will include some detailed discussions on important topics that will be useful to guide the reader through the content of this paper.

Throughout this paper we will also refer to different “tags” that are part of various APOGEE-2 data products, and we will use their official names in those files to aid the user in finding data of interest. Each time we refer to one of those “tags” we will use true-type fonts, (e.g., LOCATION_ID), and they will generally correspond to the ones present in the summary files `allStar` and `allVisit`, but they can also be found in several other APOGEE data products.

For reviewing the full description of the APOGEE data products, we refer the reader to our online documentation.⁴⁵

2.1. Concepts and Nomenclature

Fields:—The full observing program consists of a set of “fields.” A field is a particular location in the sky defined by a central coordinate and a radius that defines the field of view (FOV). Targets are then selected for fields according to specific criteria that define where holes are to be drilled in corresponding fiber optic plugplates.

Each field is uniquely identified using an integer known as the “location ID” (in the data products, LOCATION_ID). We also assign a name to each field stored in the FIELD tag that follows the naming scheme of *LLL+BB*, where *LLL* and *BB* represent the central Galactic longitude and latitude rounded to the closest integer; for example, a field centered at Galactic coordinates $(\ell, b) = (44.76, -8.64)$ would have a field name of 045–09. Some exceptions exist to this naming scheme for fields dedicated to specific astronomical objects like dwarf galaxies (e.g., with names like “CARINA” or “LMC1”) or star clusters (like “N6441”). Fields that are close to each other on the sky may have the same name, but they will always have a unique location ID.

For Contributed Programs, a suffix is added to the name that indicates the Time Allocation Committee (TAC) awarding the program. Fields from programs assigned through the CNTAC have a “-C” suffix, and fields from the OCIS TAC programs have an “-O” suffix (e.g., 000+05-C or 001+02-O). A particularly large Contributed Program allocated through OCIS that focuses on NASA’s Transiting Exoplanet Survey Satellite (TESS, Ricker et al. 2015) Southern Continuous Viewing Zone have the suffix “-O_TESS” (see Section 5.8).

Plates:—To observe our targets in APOGEE-2S, we use standard SDSS plugplates that hold the APOGEE-S fibers at the sky location of the desired target and a “plate” corresponds to the physical piece of metal used to hold the fibers at their sky positions, and each is identified with a plate ID. When drilling a design of stars into a plate, atmospheric refraction corrections need to be taken into account to calculate the positions of the

⁴⁵ https://www.sdss.org/dr16/irspec/spectro_data/

fibers on the plate and these corrections vary depending on the altitude and azimuth of the field over the night. For this reason, a “drill angle” needs to be specified for each plate, which corresponds to the hour angle (HA) at which a plate is intended to be observed; the same set of targets can occupy plates drilled to different hour angles to increase the chances that that particular design will get observed. Each plate is thus associated with a particular design and HA combination.

Design:—Each APOGEE plate includes a set of stars for observation referred to as its “design.” While multiple plates can have stars in common, even a difference of a single star implies that the design is different and would be uniquely identified with its own design ID.⁴⁶

A design is composed of one, two, or three “cohorts,” which are sets of stars restricted to a specific magnitude range. Stars are split into cohorts that receive different amounts of total exposure time such that all stars in a design will obtain roughly the same S/N over the full range of magnitudes. Bright stars are grouped into “short cohorts” (meaning that this group of stars would receive a relatively short amount of total exposure time via a smaller number of “visits” to those stars—see below), medium brightness stars into “medium cohorts”, and the faintest stars are grouped into “long cohorts” (receiving the largest amount of total exposure time).

Each design has a cohort “version,” which is a three digit number of the form *sml* where *s*, *m*, and *l* identify which of that field’s short, medium, and long cohorts (uniquely numbered starting with 1), respectively, are included in that design.⁴⁷ For example, a design for a given field that includes the second short cohort, the first medium cohort, and no long cohort would have cohort version 210. A design can, therefore, be thought of as a combination of a field and a cohort version. In their Figure 1, Z13 provides a schematic example of how different cohorts are combined into different designs and distinct plates for a single APOGEE field.

Visits:—The amount of time each star is observed is measured in units of “visits,” where a single visit corresponds to a standard length of integration of ~ 1 hour. Exposures are observed in pairs due to the need for half-pixel dithering in the spectral domain implemented for the recovery of Nyquist sampling of the native resolution delivered by the spectrograph optics onto the detectors (see Majewski et al. 2017; Wilson et al. 2019); in the Data Processing and Reduction pipeline (DRP; Nidever et al. 2015), these pairs of individually undersampled exposures are effectively blended together via interpolation to achieve proper sampling of the resolution element (for the DR16 implementation, see Jönsson et al. 2020). In the end, a standard visit corresponds to a single sequence of observations comprised of eight exposures with a dither sequence of ABBA ABBA (where A and B refer to the two nominal dither positions), which sums to a total of 4000 s (the same as for APOGEE-2N). In APOGEE-2, exceptions to this scheme were applied to those fields that contained five or more extremely faint stars ($H \gtrsim 13.5$). For these cases, the observing sequence was modified to enhance the exposure-level or visit-level S/N for these targets in a particular visit. Modifications could occur in two forms: (1) “DAB” exposures, where only a single ABBA sequence occurs with each

exposure at double length (for the same sum total exposure of 4000 s), thereby reducing the relative contribution of readnoise, and (2) “TDAB” exposures (for “triple DAB”), where an extra, double length exposure AB pair is added to the sequence for a total visit length of 6000 seconds (ABBAAB).

Plate Design:—The process of assigning targets to fibers takes into account the physical size of the fibers on the plate to avoid collisions between fibers and also considers regions in the focal plane used by each of the two acquisition cameras. Figure 1 provides an example of an APOGEE-S plate. The ferrule that contains each fiber has a diameter equivalent to $56''$ in the focal plane and this physical size sets the lower limit of allowable separation between two fibers below which they will “collide” (the fiber collision radius for APOGEE-N plates is $72''$). For initial field acquisition, central and off-axis acquisition cameras (Manta G-235B) are employed; this is different to the setup for the Northern system, which relies upon coherent fiber bundles for field acquisition.⁴⁸ These cameras are used to zero in on the central location of the pointing, determine the rotational alignment, and measure the focal plane scale. Use of these cameras creates regions that are not available for science fibers, and candidate targets at these positions are not permitted. As shown in Figure 1, these two acquisition cameras, which directly attach to the fiber plugplate, create exclusion zones in the center of the plate (with a circular footprint 5.5 in diameter) and somewhere off-axis that varies with each plate (with a rectangular footprint occupying an area equivalent to approximately $10' \times 7'$). Though the physical plates in the South are the same physical size as the plates for APOGEE-N, due to differences in the telescope plate scales, the APOGEE-S plates cover a smaller area than APOGEE-N. Ignoring the above exclusion zones, the maximal FOV of an APOGEE-S plate is 2.8 deg^2 (corresponding to a 1.9 diameter), compared to the 7.1 deg^2 FOV for APOGEE-N (corresponding to a 3.0 diameter; for a discussion of maximal FOV versus the drillable FOV, see Section 2.1 of Z17). To see other differences between the APOGEE-N and APOGEE-S plates, compare Figure 1 here to Figure 13 in Majewski et al. (2017).

2.2. Targeting Bits

Like APOGEE-1, APOGEE-2 uses target flags to indicate the reason why each target was selected for observation; the flags are encoded using bitmasks in the data products. These flags are set to help reconstruct the target selection function of the survey. Note, however, that use of these flags may not allow for the complete retrieval of a desired set of stars. As one example, stars selected for observation because they are red clump (RC) candidates have bit 25 set in APOGEE2_TARGET2, but a large number of RC stars are serendipitously included in our sample, and hence, will not have that bit set.

The APOGEE-2 targeting bit labels are APOGEE2_TARGET1, APOGEE2_TARGET2, APOGEE2_TARGET3, and, the recently defined APOGEE2_TARGET4. Currently, APOGEE2_TARGET4 has no assigned bits, but we anticipate that it will be used for the final APOGEE-2 data release (DR17). Table 1 provides a summary of all APOGEE-2 targeting bits for both APOGEE-2N and APOGEE-2S. In the following section, we

⁴⁶ The Design IDs are only found in Intermediate Data Products; see https://www.sdss.org/dr16/irspec/spectro_data/.

⁴⁷ The cohort versions are only found in Intermediate Data Products; see https://www.sdss.org/dr16/irspec/spectro_data/.

⁴⁸ The APOGEE-N plates have a central region of $96''$ that cannot be used for targets due to a post that supports the plate; see Owen et al. (1994).



Figure 1. Example of an APOGEE-2S plate. APOGEE-S plates cover a smaller area on the sky than APOGEE-N plates (due to telescope plate scale differences), and they also have a slightly different layout (compare to Figure 13 in Majewski et al. 2017). Most obviously, there is a central hole for an on-axis acquisition camera and another rectangular hole for an off-axis camera. These fiber exclusion regions are taken into account in the target selection and plate design software. Another difference with APOGEE-N plates is that all plate markings, including coding of the holes to denote bright, medium, and faint fibers, are automatically printed for the APOGEE-S plates, whereas they are hand-marked for the APOGEE-N plates (the coding may not be visible without enlarging the image). Photo by R. Beaton.

provide brief descriptions of the major modifications to the Targeting Bits that were given in Z17.

2.3. Targeting Flag Changes

In the middle of 2020, the APOGEE-2 team reviewed all targeting flags to ensure the consistency of their application for APOGEE-2 targeting. In the course of this process, we fixed some flags that were set incorrectly for certain classes of stars, added new targeting flags, and slightly modified some of the flag definitions to match better how they were used.

In Table 1, we present all of the APOGEE2_TARGET1, APOGEE2_TARGET2, and APOGEE2_TARGET3 flag bits and their descriptions. All of the target flags that are new or different from those presented in Z17 are shown in bold face.

Below, we list all of the APOGEE-2 related targeting flags that were modified, either in their definition or in their implementation. Those flags that are highlighted in Table 1

but are not listed in this section are new flags that have been defined since Z17 but were only used for APOGEE-2N, with their descriptions given in R. Beaton et al. (submitted; AAS29028). The one exception is APOGEE2_TARGET1=6, which was used for K2 targeting and is described in Section 4.7.

APOGEE2_TARGET1 = 29: “Faint” target.

Even though this flag was defined prior to the review, it had only been used for a small group of targets for which it was set “manually” in plate design. To make this flag consistent with its description, we systematically compared the H magnitudes of stars with the number of visits they were planned to receive. We then flagged all stars that had fewer visits planned than what they needed to reach the nominal S/N value lower limit of 100 in Table 2. We highlight that there is a type of stars in our sample called “special target” (see Section 3.3.2) for which this flag was not set because the S/N goals associated with those stars is, on occasion, different from the ones for the rest of our sample.

Table 1
APOGEE-2 Targeting Bits

| APOGEE2_TARGET1 | | APOGEE2_TARGET2 | | APOGEE2_TARGET3 | |
|-----------------|--------------------------------------|-----------------|---|-----------------|--|
| Bit | Criterion | Bit | Criterion | Bit | Criterion |
| 0 | Single $(J - K_s)_0 > 0.5$ bin | 0 | K2 GAP Program | 0 | KOI target |
| 1 | “Blue” $0.5 < (J - K_s)_0 < 0.8$ bin | 1 | California Cloud Target | 1 | Eclipsing binary |
| 2 | “Red” $(J - K_s)_0 > 0.8$ bin | 2 | Abundance/parameters standard | 2 | KOI control target |
| 3 | Dereddened with RJCE/IRAC | 3 | RV standard | 3 | M dwarf |
| 4 | Dereddened with RJCE/WISE | 4 | Sky fiber | 4 | Substellar companion search target |
| 5 | Dereddened with SFD $E(B - V)$ | 5 | External survey calibration | 5 | Young cluster target |
| 6 | No dereddening | 6 | Internal survey calibration (APOGEE-1+2) | 6 | K2 Star |
| 7 | Washington+DDO51 giant | 7 | Outer Disk Substructure Member | 7 | APOGEE-2 Target |
| 8 | Washington+DDO51 dwarf | 8 | Outer Disk Substructure Candidate | 8 | Ancillary target |
| 9 | Probable (open) cluster member | 9 | Telluric calibrator | 9 | Massive Star |
| 10 | Globular Cluster Candidate | 10 | Calibration cluster member | 10 | ... <i>QSOs</i> |
| 11 | Short cohort (1–3 visits) | 11 | K2 Planet Host | 11 | ... <i>Cepheids</i> |
| 12 | Medium cohort (3–6 visits) | 12 | ... <i>Kepler Synchronized Binaries</i> | 12 | ... <i>The Distant Disk</i> |
| 13 | Long cohort (12–24 visits) | 13 | Literature calibration | 13 | ... <i>Emission Line Stars</i> |
| 14 | Random sample member | 14 | Gaia-ESO overlap | 14 | ... <i>Moving Groups</i> |
| 15 | MaNGA-led design | 15 | ARGOS overlap | 15 | ... <i>NGC 6791 Populations</i> |
| 16 | Single $(J - K_s)_0 > 0.3$ bin | 16 | Gaia overlap | 16 | ... <i>Cannon Calibrators</i> |
| 17 | No Washington+DDO51 classification | 17 | GALAH overlap | 17 | ... <i>Faint APOKASC Giants</i> |
| 18 | Confirmed tidal stream member | 18 | RAVE overlap | 18 | ... <i>W3-4-5 Star-forming Regions</i> |
| 19 | Potential tidal stream member | 19 | APOGEE-2S commissioning target | 19 | ... <i>Massive Evolved Stars</i> |
| 20 | Confirmed dSph member (non Sgr) | 20 | Halo Member | 20 | ... <i>Extinction Law</i> |
| 21 | Potential dSph member (non Sgr) | 21 | Halo Candidate | 21 | ... <i>Kepler M Dwarfs</i> |
| 22 | Confirmed Mag Cloud member | 22 | l-m target | 22 | ... <i>AGB Stars</i> |
| 23 | Potential Mag Cloud member | 23 | Modified bright limit cohort ($H > 10$) | 23 | ... <i>M33 Clusters</i> |
| 24 | RR Lyrae star | 24 | Carnegie (CIS) program target | 24 | ... <i>Ultracool Dwarfs</i> |
| 25 | Potential bulge RC star | 25 | Chilean (CNTAC) community target | 25 | ... <i>SEGUE Giants</i> |
| 26 | Sgr dSph member | 26 | Proprietary program target | 26 | ... <i>Cepheids</i> |
| 27 | APOKASC “giant” sample | 27 | N-CVZ OBAF stars | 27 | ... <i>Kapteyn Field SA57</i> |
| 28 | APOKASC “dwarf” sample | 28 | N-CVZ GI Programs | 28 | ... <i>K2 M Dwarfs</i> |
| 29 | “Faint” target | 29 | N-CVZ CTL star | 29 | ... <i>RV Variables</i> |
| 30 | APOKASC sample | 30 | N-CVZ Giant with RPMJ | 30 | ... <i>M31 Disk</i> |

Notes.

Note 1: A new bitmask, APOGEE2_TARGET4, has been added to the data model for DR17 but is currently unpopulated.

Note 2: Flags that are new or different from those presented in Z17 are highlighted in bold.

Table 2
Cohort Visits and Magnitude Limits

| NVisits | H_{\min} [mag] | H_{\max} [mag] |
|---------|---------------------|---------------------|
| 1 | 7.0 | 11.0 |
| 3 | 11.0 | 12.2 |
| 6 | 12.2 | 12.8 |
| 12 | 12.8 | 13.3 |
| 24 | 13.3 | 13.8 |

APOGEE2_TARGET2 = 16: Gaia overlap.

This flag was originally designed to flag any stars that overlapped with the Gaia observations. However, no stars were intentionally targeted because of their overlap with Gaia, and thus, this flag did not serve to identify a reason for why specific stars were targeted. Moreover, given that Gaia is photometrically complete well beyond APOGEE-2’s faintest magnitude limits, such a flag would nominally include nearly all of APOGEE-2’s targets. In addition, a Gaia cross-match is already presented along with APOGEE-2 data products (e.g., for DR16 a cross-match to Gaia DR2; Jönsson et al. 2020, and for DR17 a cross-match with EDR3, J. A. Holtzman et al. 2021, in preparation), providing a clearer way to identify the overlap between Gaia and

APOGEE. For all of these reasons, we changed the meaning of this targeting flag, which now identifies targets that explicitly used Gaia data (almost exclusively proper motions) for the target selection process, and we have set this flag only for those stars.

APOGEE2_TARGET1 = 10: Globular Cluster Candidate.

This is a new flag used for globular cluster candidates that were selected either by photometry only or by membership probabilities based on proper motions. At the time of their selection no such flag existed, so targets selected as Globular Cluster candidates were not identified in any way. This has now been remedied.

APOGEE2_TARGET2 = 0: K2 GAP Program.

This is a new flag defined to identify targets selected because they were part the K2 Galactic Archaeology Program (GAP; Stello et al. 2017). Most of these stars were already flagged with APOGEE2_TARGET3 = 6, which is used for all K2 targets, but now all K2 targets, additionally, have flags associated with their corresponding priority groups, which are listed in Section 4.7.

APOGEE2_TARGET2 = 20: Halo Members.

This flag was previously used to identify halo targets specifically selected as part of the APOGEE-2N Bright Time eXtension (BTX). Now we have extended the meaning of this flag to include a similar class of stars in APOGEE-2S that were

Table 3
Color Cuts for Galactic Regions

| Galactic Region | ℓ Range | b Range | Color Selection ^a [mag] | Targeting Flag in APOGEE2_TARGET1 ^b | |
|-----------------|--------------------------------------|-----------------|---------------------------------------|--|---------------------------|
| | | | | bit | Description |
| Bulge | $<20^\circ$ or $>340^\circ$ | $<25^\circ$ | $0.5 \leq (J - K_s)_0$ | 0 | APOGEE2_ONEBIN_GT_0_5 |
| Disk | $\geq 20^\circ$ and $\leq 340^\circ$ | $<25^\circ$ | $0.5 \leq (J - K_s)_0 < 0.8$ | 1 | APOGEE2_TWOBIN_0_5_TO_0_8 |
| | | | $0.8 \leq (J - K_s)_0$ | 2 | APOGEE2_TWOBIN_GT_0_8 |
| Halo | no ℓ limits | $\geq 25^\circ$ | $0.3 \leq (J - K_s)_0$ | 16 | APOGEE2_ONEBIN_GT_0_3 |

Notes.

^a The values for a star are coded in the MIN_JK and MAX_JK tags.

^b The equivalent bit for APOGEE-1 is APOGEE1_TARGET1 and it follows the same definitions.

selected using information from the SkyMapper survey (Keller et al. 2007); see Section 4.3.1.

APOGEE2_TARGET2 = 21: Halo Candidates.

This flag was originally defined to be used for stars from the APOGEE-2N BTX, but it now also includes halo candidates from APOGEE-2S that were selected using Gaia proper-motion information (Section 4.3.1).

3. Targeting Selection Overview

For APOGEE-2, the 300 fibers of each APOGEE spectrograph are divided among 250 science targets, 35 sky targets, and 15 telluric targets.⁴⁹ This section provides an overview of how each of these targets types are selected.

3.1. Telluric Absorption Calibration Targets

The wavelength range of the APOGEE spectrographs contains a number of contaminant spectral features from the Earth’s atmosphere. To measure the telluric absorption we need to observe stars whose spectra are as close as possible to a featureless blackbody, and thus, we select the stars with the bluest observed $J - K_s$ colors in each field for this purpose. The spectra of these stars are processed by the APOGEE data reduction pipeline to make the telluric corrections (apred; Nidever et al. 2015; Holtzman et al. 2018; Jönsson et al. 2020). To take into account angular variations in the telluric absorption during observations, telluric calibrators are spatially distributed across the plugplate as homogeneously as possible. For this purpose, the FOV for each field is divided into a number of segmented, equal-area zones (Figure 8 of Z13 provides a zone schematic). These stars are the first ones selected for APOGEE-2S plates and can be identified with bit 9 in APOGEE2_TARGET2.

3.2. Sky Contamination Calibration Targets

The APOGEE data reduction pipeline uses observations of “empty” sky regions to monitor the airglow and other foreground and background emissions. To select sky targets in a field, we first select candidate positions that correspond to locations that have no 2MASS sources within a $6''$ radius. Then, as we do for selecting telluric absorption calibrators (Section 3.1), the plugplate FOV is split into equal-area zones (Figure 8 of Z13 provides a zone schematic) and we select up to eight candidate positions for each zone, to create the final list of sky positions. These fibers are the third and last type of targets selected in APOGEE plates. Sky positions will have bit

⁴⁹ APOGEE-1 used 230 fibers for science targets, 35 for sky targets, and 35 for telluric targets. See Z17 for the motivations for this change.

4 set in APOGEE2_TARGET2, but typically these spectra are not kept throughout the reduction process.

3.3. Science Target Selection

Our science programs are designed to address many distinct scientific goals, which can require targeting specific Galactic subcomponents or specific stellar types. The subsections that follow explain the most important aspects of the science target selection process.

In the process of filling an APOGEE plate with the different classes of targets, science targets are selected after telluric correction targets but before sky targets are selected. There are two major types of science targets in APOGEE, the “main red star” sample, which is randomly selected to map the bulge, disk, or halo based on apparent magnitude and color values, and “special targets”, which correspond to specific high-priority targets (e.g., red clump, stream members, RR Lyrae stars). In this latter class, targets can be selected using complex combinations of photometric, chemical, and kinematical information.

“Special targets” have top priority and then the “main red star” sample is the source for all remaining fibers. In the following subsections, we explain how these two types of stars are selected.

3.3.1. Main Red Star Sample

The “main red star” sample comprises the majority of the APOGEE-2S stars by number. The underlying targeting strategy for this sample is a simple color–magnitude criterion to select stars from the bulge, disk, and halo (these are given in Table 3).

To select targets for the “main red star” sample, we start with all of the objects in the 2MASS Point Source Catalog (PSC; Skrutskie et al. 2006) that fall in the FOV of a given field. The NIR photometry is complemented by mid-IR photometry from either the Spitzer+IRAC GLIMPSE (Benjamin et al. 2005; Churchwell et al. 2009) or the AllWise (Wright et al. 2010) catalogs. The Rayleigh–Jeans Color Excess method (RJCE) is then used to estimate the line-of-sight extinction for each individual target (Majewski et al. 2011; Zasowski et al. 2013, 2017; also discussed below). Data quality limits are applied to ensure that the sources have small magnitude uncertainties and reliable quality photometry flags (for the specifics, we refer the reader to Table 2 of Z17).

To maximize the number of giant stars targeted while ensuring a simple selection function, we apply a simple color selection using the dereddened $(J - K_s)_0$ color. For most APOGEE fields, we use the RJCE method to estimate $E(J - K_s)$; (Majewski et al.

2011); RJCE assumes that, for filters sampling the Rayleigh–Jeans tail of stellar spectra, all stars nominally have the same color such that any deviation from that baseline color (in this case we adopt the $(H - I_2)$ or $(H - W_2)$ indices) is due to foreground dust. RJCE is used for the main red star sample in nearly all disk and bulge fields.

RJCE is known to be less reliable when the total $E(J - K_s)$ is of order the color uncertainty in a given field; more specifically, for fields with low extinction that are well out of the Galactic plane (e.g., the typical uncertainty on $(H - W_2)$ is larger than the extinction in these fields). To avoid the overestimation of $E(J - K_s)$ for low extinction halo fields, the reddening was determined using the dust maps from Schlegel et al. (1998).

Because multiple dereddening methods are used, the targeting flags indicate the method adopted for a given target. More specifically, the dereddening method used for each target is indicated by the APOGEE2_TARGET1 flags recorded in: bit 3 for RJCE using Spitzer+IRAC, bit 4 for RJCE using the Wide-field Infrared Survey Explorer (WISE), bit 5 using Schlegel et al. (1998), or bit 6 if no dereddening was applied to that target. In addition to the targeting flags, the summary files contain a number of convenience tags that provide the values used for extinction; these include AK_TARG for the A_K used in targeting, AK_TARG_METHOD with a string defining the method, AK_WISE with the all-sky RJCE value from WISE photometry, and SFD_EBV with the all-sky value from Schlegel et al. (1998).⁵⁰ The appropriate 2MASS, WISE, and Spitzer photometry, when available, is also provided in the summary files.

The color criteria for selecting red stars in a given field depends on the Galactic component being targeted; these criteria are summarized in Table 3. The color selection strategy employed for each target is indicated in the APOGEE2_TARGET1 flag by bit 0 for $(J - K_s)_0 > 0.5$, bit 1 for the “blue” bin of $0.5 \leq (J - K_s)_0 < 0.8$, bit 2 for the “red” bin of $(J - K_s)_0 > 0.8$, and, bit 16 for $(J - K_s)_0 > 0.3$.

For some fields targeting the halo ($|b| \geq 25^\circ$), we apply an additional photometric criterion designed to distinguish between dwarf and giant stars of the same spectral type. This classification is performed by combining the Washington filter system with the DDO51 filter (hereafter W+D), an intermediate-band filter that spans the surface gravity sensitive Mg b feature in the spectra of cool stars, to construct a color–color diagram, $(M - T_2)$ against $(M - \text{DDO51})$. Because of the gravity sensitivity of the DDO51 filter (McClure 1973) and the T_{eff} sensitivity of the Washington filters (here M and T_2 ; Cantana 1976), this color–color space provides an effective means of selecting likely giants even in dense foregrounds (e.g., Geisler 1984; Majewski et al. 2000; Muñoz et al. 2005). Z13 (Z17) provides a detailed discussion of how this photometry is used for APOGEE-1 (APOGEE-2) targeting. This same methodology is used for the APOGEE-2S targeting when W + D photometry was available (the photometry and its application are discussed in Z17). When assigning priorities to the targeting in halo fields that have W + D photometry, the first priority were W + D selected giants, then stars with no W + D classification, and lastly, W + D classified dwarfs were used to fill remaining fibers.

⁵⁰ For additional description, please see the data model here: https://data.sdss.org/datamodel/files/APOGEE_ASPCAP/APRED_VERS/ASPCAP_VERS/allStar.html.

Finally, to attain a goal S/N of 100 per pixel in the spectra, magnitude limits must be set on the targets that are selected for each design. Because each field design has short, medium, or long cohorts that receive different numbers of visits, the magnitude limits applied to the cohorts are modified according to the number of visits that each cohort will receive (following Table 2). The total number of visits for a field is typically equivalent to the number of visits planned for the longest cohort (i.e., faintest target) included in its designs.

3.3.2. Special Targets

Some APOGEE-2S fields are designed with special scientific goals in mind and, therefore, include a list of specific stars to be targeted at the highest priority, which we refer to broadly as “special targets.” Typically, “special targets” are provided by a specific Science Working Group in prioritized lists. In some cases, the “special targets” for an APOGEE-2S field may use all of the available fibers, as in the Large Magellanic Cloud program, while other programs only require a handful of fibers, as in the Open Cluster program. Any remaining, unallocated fibers are used to bolster the “main red star” sample.

The Working Group for each APOGEE-2S program sets their own criteria to select high-priority targets; Table 4 provides a brief summary of these programs. Details about the original selection method used for all APOGEE-2S programs is described in Z17. Stars that were selected as different types of “special targets” can also be identified according to their set targeting bits (Table 1).

4. Changes to the Main Survey

In this section we detail all of the changes made to the targeting strategy, which includes the target selection and field locations of APOGEE-2S, with respect to the original plan given in Z17. Section 4.1 provides the motivation for these changes and, in particular, contains an overview of the time allocation for APOGEE-2S. After this overview, the subsections that follow are organized by APOGEE-2S science program and describe the changes applied to the targeting strategy.

4.1. Motivation

One of the main motivations for this paper is to describe modifications to the original APOGEE-2S survey strategy described in Z17. These modifications occurred for three reasons: (1) internal evaluations via Targeting Reviews, using our “Lessons Learned” from APOGEE-N, of whether the survey strategies in place would enable APOGEE-2S to achieve its scientific goals, (2) the advent of new data from surveys outside of SDSS (e.g., Gaia) that could significantly enhance APOGEE targeting efficiency, and (3) modifications to the main survey plan due to alterations in the observing schedule.

Internal evaluations of all APOGEE-2 programs occurred on an approximately yearly basis. For some scientific programs, the review suggested that a modification to the original targeting strategy was needed to meet the science goals, or that the program would significantly benefit from considering additional aspects for the target selection process. In other cases, the sky efficiency was either lower or higher than originally estimated; this particularly occurred at some local sidereal time (LST) windows for which the weather was better than our adopted weather model.

Table 4
Summary of APOGEE-2S Main Survey Programs

| Name | Total Fields | Total Visits | Section | Special Target Flags | Systems Included | Additional References (if applicable) | PROGRAMNAME |
|-------------------|--------------|--------------|---------|---|---|--|--|
| Bulge | 56 | 347 | 4.2 | ... | ... | Z17 | bulge |
| Disk | 78 | 579 | ... | ... | ... | Z17 | disk, disk1, disk2 |
| Halo | 15 | 126 | 4.3.1 | Target1 = 18 Target2 = 20,21 | Halo stars, Sagittarius stream, Orphan stream | Z17 for main red star sample; Hayes et al. (2018b) for Sagittarius stream targets | halo, halo2_stream |
| Streams | 26 | 132 | 4.3.2 | Target1 = 18,26 Target2 = 20,21 | Jhelum stream, Sagittarius stream, Orphan stream | ... | sgr_tidal, stream_halo, stream_disk |
| Open Clusters | 15 | 87 | 4.6 | Target1 = 9 | Berkeley 75, Berkeley 81, M 8, M 16, M 67, NGC 2204, NGC 2243, NGC 6253, NGC 5999, NGC 6583, NGC 6603, Trumpler 20, Trumpler 32, Tombaugh 2, Collinder 261 | Donor et al. (2018) | cluster_oc |
| Globular Clusters | 20 | 147 | 4.8 | Target1 = 10 Target2 = 2,10 | 47 Tucanae, M 10, M 12, M 22, M 4, M 55, M 68, M 79, NGC 1851, NGC 2808, NGC 288, NGC 2298, NGC 3201, NGC 362, NGC 6388, NGC 6397, NGC 6441, NGC 6752, Omega Centauri | ... | cluster_gc |
| Magellanic Clouds | 48 | 483 | 4.5 | Target1 = 22,23 | LMC, SMC | Nidever et al. (2020) | magclouds |
| Dwarf Spheroidals | 4 | 96 | 4.4 | Target1 = 20,21 | Carina, Sextans, Sculptor, Fornax | Z17 | halo_dsph |
| Sagittarius | 6 | 36 | ... | Target1 = 26 Target2 = 10 | Sagittarius dwarf core | ... | sgr |
| K2 | 87 | 87 | 4.7 | Target1 = 30 Target2 = 0,11 Target3 = 6,28 | K2 Campaigns: C6, C8, C10, C14, C15, C17 | R. Beaton et al. (submitted; AAS29028) | k2 |

6

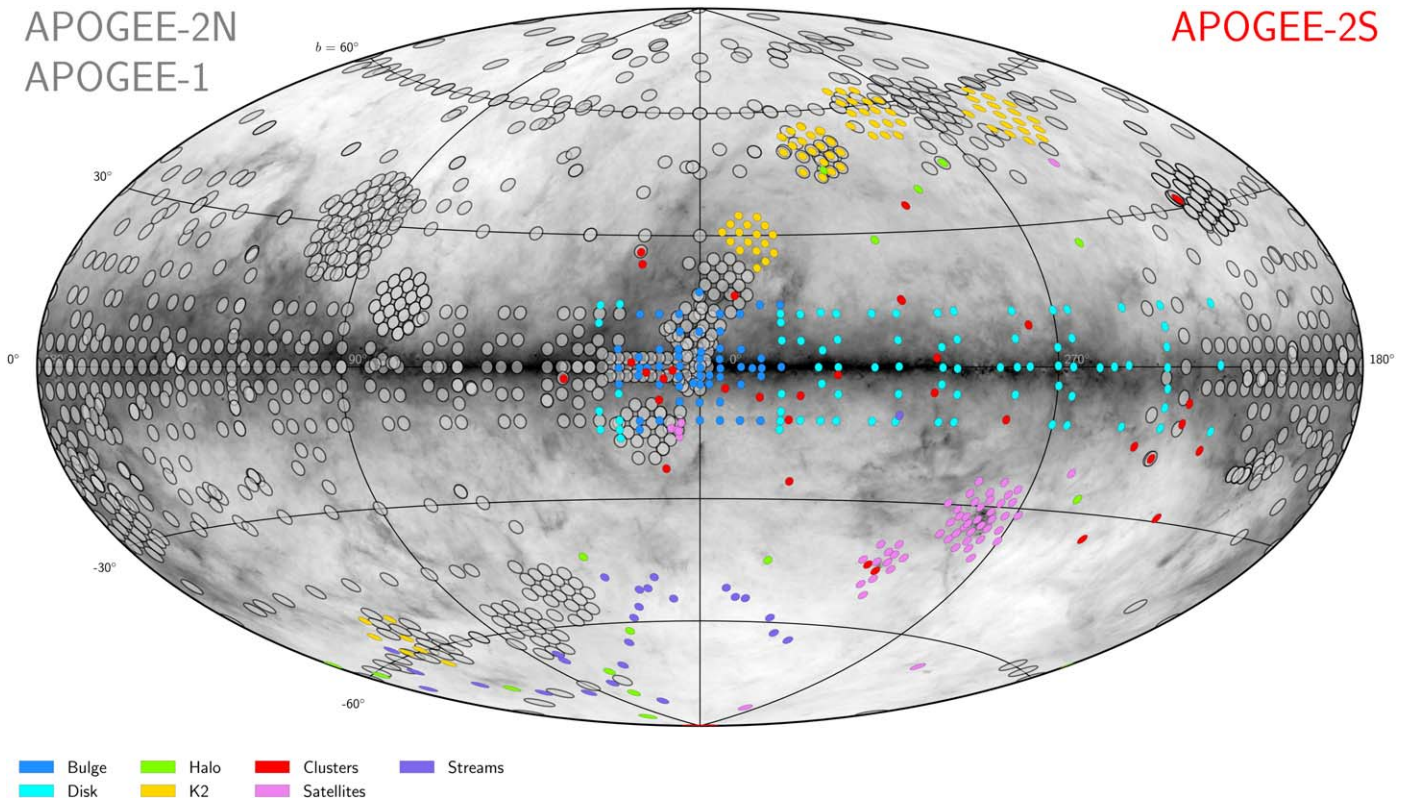


Figure 2. Final APOGEE field plan in Galactic coordinates with APOGEE-2S fields from the main survey highlighted in color. The color coding corresponds to the scientific program affiliated with the field. The background image corresponds to the dust map from Schlegel et al. (1998). For completeness, we also show the other components of the APOGEE survey (APOGEE-1 and APOGEE-2N) as gray semi-transparent circles. The meridians are spaced every $\Delta l = 90^\circ$ and the parallels are spaced every $\Delta b = 30^\circ$.

Additional motivations for modifying the targeting strategy came by way of previously unavailable information from space-based missions like Gaia (Gaia Collaboration et al. 2016a, 2016b, 2018), the K2 mission of the Kepler spacecraft (Howell et al. 2014), or TESS (Ricker et al. 2015), as well as complementary ground-based surveys like GALAH (Zucker et al. 2012), SkyMapper (Keller et al. 2007), or RAVE (Steinmetz et al. 2006; Kunder et al. 2017).

Finally, modifications to the APOGEE-2S observing schedule occurred both because of the addition of some nights to the originally expected allocation or shifts in the scheduled time. This schedule was then modified for two main reasons: a delay in commissioning from 2016 August to 2016 October and a forced and lengthy closure of Las Campanas Observatory due to the COVID-19 pandemic near the end of the survey. The total observing hours and their distribution throughout the year determine the total number of visits we expect to observe at each LST, and thus, are crucial for estimating the fields that we will be able to observe. All of these factors were considered simultaneously to design and implement modifications to what became a somewhat dynamic targeting scheme, but one that always pointed at maximizing scientific return.

In the end, a total of 352 nights were allocated for the Main Survey programs⁵¹ from 2017 April to 2021 January. More details about the allocation of du Pont 2.5 m time to the APOGEE project will be given in the forthcoming APOGEE-2 overview paper (S. Majewski et al. 2021, in preparation).

⁵¹ With 10 nights in 2017 used for the commissioning of the APOGEE-S spectrograph, which are not counted toward the Main Survey observing total.

The final field map for the APOGEE-2S Survey is given in Figure 2, where we show the positions, in Galactic coordinates, for all of the Main Survey APOGEE-2S fields. The fields in APOGEE-2S are color coded by their science program. We also show in gray circles the APOGEE-1 and APOGEE-2N fields to exhibit the overall coverage of the APOGEE survey. This figure shows how APOGEE-2S makes APOGEE a truly panoramic survey reaching all regions and components of the Milky Way by covering regions inaccessible from the Northern Hemisphere, most notably the inner Galactic regions.

4.1.1. Observing Efficiency of APOGEE-2S and Resulting Modification to Visit Plan

The observing efficiency of APOGEE-2S was continuously calculated during survey operations and compared to the initial estimate used for the Z17 plan. The original observing plan of the survey was constructed assuming a seasonally averaged observing efficiency of ~ 4.7 visits per night, and involved 1493 visits planned to be observed over the entire APOGEE-2S survey period from 2017 February to 2020 June.

During the first year of the survey (2017), operational strategies were under development and initial plate delivery timescales were sometimes mismatched to the optimal observation dates. This translated to miscalculations of the visits expected per LST for the first plateruns, which in turn resulted in nights that had some unused visits because there were no suitable plates. Additionally, confronted with a completely new instrument and a still evolving observing infrastructure that had many significant differences with that in place for decades at APO, the APOGEE-2S engineering and

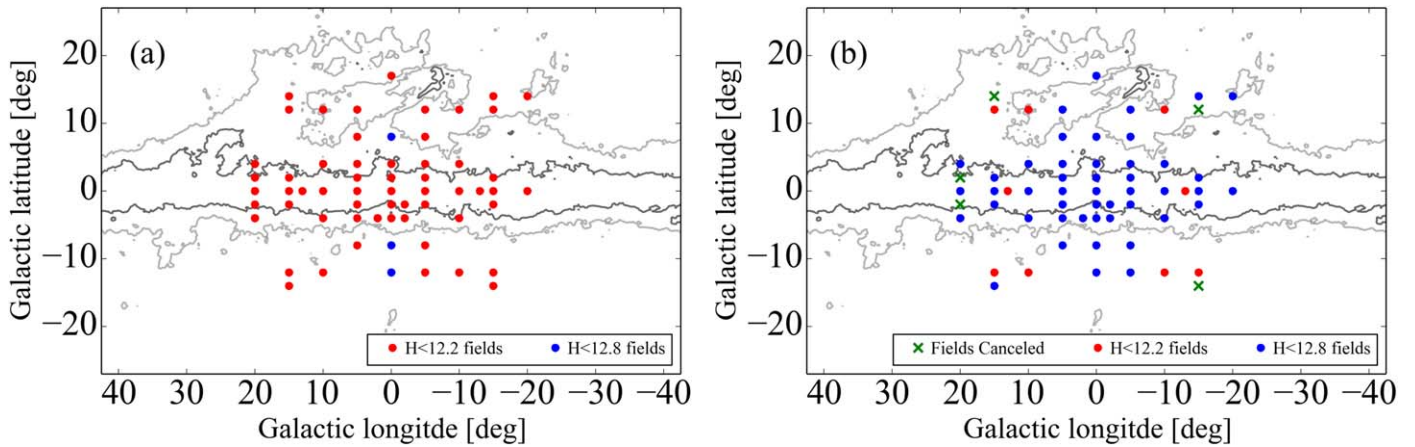


Figure 3. The APOGEE-2S coverage and depth plan for the Galactic bulge. The full Galactic bulge region is shown with medium (red) and long (blue) fields indicated. Gray contours show color excess $E(B - V)$ levels of 0.5 (inner line) and 1.5 (outer line). (a) The original plan, which was composed of 3 visit fields to a depth of $H \sim 12.2$ (red), with three deeper pointings at $\ell = 0^\circ$ (blue). (b) The final plan, which demonstrates the increase in fields reaching $H \sim 12.8$ (blue) and the elimination of some fields (black crosses), as well as the fields that were properly designed for $H \sim 12.2$ that were unchanged. As discussed in the text, the result of these modifications to the survey is that our mapping of the Galactic bulge goes deeper and has built a larger sample of bona fide bulge stars (see, e.g., Rojas-Arriagada et al. 2020; Hasselquist et al. 2020).

observing teams took some time to optimize operational strategies and software and to become proficient in their use. Together, these factors translated to a lower than expected efficiency of ~ 3.1 visits per night during that year (65% of the anticipated efficiency). These initial challenges, however, were solved and, for 2018 and the first half of 2019, the observing efficiency grew to ~ 5.8 and ~ 5.5 visits per night, respectively (123% and 117% of the anticipated efficiency).

Assuming that the observing efficiency would remain constant until the end of the survey, we re-estimated that our overall observing efficiency would be ~ 5.0 visits per night. Using this new efficiency, we concluded that in our total APOGEE-2S nights we would be able to observe ~ 224 visits more than our original expectations. For this reason, the original field plan was modified from a 1493 visit plan to one containing 1717 total visits. From these extra visits 58 (26%) were necessary to account for the modifications made to the Bulge and RRL Programs, while the others were used to observe new fields that were not in the original targeting plan.

4.1.2. COVID-19 Shutdown and Final Plan

Due to the COVID-19 pandemic’s global spread in early 2020, LCO shut down all operations in mid-March 2020. This included APOGEE-2S, which had to stop operations about 6 months before the nominal conclusion of the APOGEE-2S survey. Ultimately, this resulted in a loss of 77 originally planned APOGEE-2S nights. When LCO reopened in 2020 October, APOGEE-2S was granted an extension that encompasses the original 77 nights lost due to the COVID-related closure as well as 11 additional nights.

The total APOGEE-2S extension period includes 88 nights over the 2020 October 20–2021 January 21 time frame. While this extension allowed APOGEE-2S to (more than) recover its lost time, the allocated nights gave very little access to the same portion of the sky, which necessitated a major overhaul of the plan for the remainder of the survey, with modified objectives to make compelling use of the altered sky access. The most notable impact on the survey was a loss of almost the entire final year (i.e., about 1/3) of the planned APOGEE observations of the central Milky Way.

The COVID-19 extension left a projected 403 visits to fill with newly drilled plates, but a short time line in which to produce them, and with the imminent danger that any resumption of operations might be tentative. Under such circumstances, it was decided that the most expeditious path forward was to expand those APOGEE-2S programs already primarily focused on those regions of the sky—namely the Magellanic Cloud and the Galactic Halo Programs, both of which would not only benefit from greater coverage, but could also be flexible in the event of additional closures or extensions. With the extra 403 visits from the COVID-19 extension the APOGEE-2S observing plan reached its definitive version, consisting of 2120 visits, spread over 352 nights, whose sky coverage is shown in Figure 2. In the end, despite numerous obstacles the survey had overcome, the size of the final observing plan represents an increase of $\sim 42\%$ with respect to the original 1493 visit plan, albeit with some shift in emphasis from that originally envisioned.

The following sections present all of the changes to the APOGEE-2S observations originally planned and presented in Z17. The presentation is organized by scientific program.

4.2. The Milky Way Bulge

In May 2018, when the second of our four total bulge seasons was starting we discovered that, due to an error in the execution of the targeting selection software, a significant fraction of the plates in the Bulge Program contained stars fainter than the originally intended magnitude limit for the plate (e.g., see Table 2). In this subsection, we will briefly explain the origin of this problem, the actions taken to resolve it, and how the implemented solution, along with an increased observing efficiency, fortuitously resulted in a deeper, more complete survey of the Galactic bulge than originally planned.

4.2.1. The Problem

The spatial distribution of the fields in the Bulge Program is given in Figure 3, which shows the original plan (Figure 3(a)) and the final plan (Figure 3(b)). The color coding in Figure 3 indicates the targeting depth of either $H = 12.2$ ($S/N = 100$ in

3 visits; red) or $H = 12.8$ ($S/N = 100$ in 6 visits; blue). The intended Bulge Program (Figure 3(a); Z17) was to sample the bulk of the Galactic bulge region in a grid with plates going to $H = 12.2$ depth, with a handful of deeper fields at strategic locations designed to complement the APOGEE-1 Bulge Program (Z13). However, the Bulge Program that was implemented in the target selection software is shown in Figure 3(b); the latter reflects the fact that the majority of the bulge fields were inadvertently drilled with stars as faint as $H = 12.8$ (blue) and, given that observations had already begun, the options to resolve the problem were limited. Were the nominal survey minimum S/N requirement enforced, completion of the observing plan shown in Figure 3(b) would have required about twice as much time as was available for the Bulge Program.

More specifically, the original Bulge Program (Figure 3(a)) contained 34 fields meant to be observed with 3 plates each. Each of the fields included three short cohorts scheduled for 1 visit each and a single medium cohort scheduled for 3 visits (in the cohort nomenclature introduced earlier, a “310 plate”). Ten of the bulge fields were intended to have 6 visits total, but in order to observe more of the stars in these dense bulge fields, they were intended to have a 3 visit depth like the above fields, having two pairs of 3 visit medium cohorts and six 1 visit short cohorts (e.g., a 620 cohort complement, with two sets of 310). In both the 3 visit and 6 visit fields, the 1 visit short cohorts were erroneously filled with stars as faint as $H = 12.2$ (i.e., what is normally a 3 visit depth) and some of the 3 visit cohorts were filled with stars as faint as $H = 12.8$ (i.e., the normal 6 visit depth). This is problematic for APOGEE observations, because, in 1 visit, the faintest stars in the short cohorts would be expected to achieve $S/N \sim 58$ and, in 3 visits, the faintest stars in the medium cohorts should reach $S/N \sim 75$ —i.e., neither cohort satisfying the APOGEE goal of $S/N = 100$ for all targets.⁵²

While the fields just described formed the bulk of the bulge design problem, there were other bulge fields where the magnitude limits were properly set given the scheduled number of visits, and a few fields where the number of visits was larger than needed to reach $S/N = 100$. However, the overall bulge field plan was erroneously created, because achieving S/N of 100 in all of these fields would have required considerably more observing time than was available. Therefore, we needed a mitigation strategy.

4.2.2. The Solution

By the time this situation was discovered, the first out of our four total bulge seasons was complete and we had already designed and drilled all of the plates for the second season. This means that by that moment a significant fraction of the problematical plates had already been drilled, and some were even observed. For that reason, re-designing, re-drilling, and re-shipping these plates with the aim of restoring the original plan was deemed impractical, and a solution was sought that optimized utilizing the plates already in hand. This required finding a compromise between S/N needs and other modifications that made optimal use of the available, bulge-accessible observing nights for APOGEE-2S.

The solution that was devised involved the following action items:

1. Cancel all pending visits to plates that would yield $S/N > 100$ for the faintest stars on the plate. The three fields involved correspond to those indicated by blue circles in Figures 3(a) and (b).
2. Cancel visits for the second set of three plates for the 6 plate fields (i.e., remove the second 310 cohort set from a 620 cohort complement field). Because there are no common stars between the two sets of medium cohorts (and all 1 visit cohorts are distinct), canceling one set does not affect the S/N of the stars in the other set. This change maintains our spatial coverage, but with a smaller total sample in those fields.
3. Cancel fields from bulge regions that had another field nearby and/or a field symmetric with respect to the $\ell = 0^\circ$ axis. These five fields are indicated with an “x” marker in Figure 3(b).
4. Increase the number of total visits for cohorts whose faintest stars are $H \sim 12.2$ stars from 1 visit to 2 visits. This change ensures that all targets reach $S/N > \sim 80$. These stars have been flagged as “Faint” targets with targeting flag APOGEE2_TARGET1 = 29.
5. Increase the number of total visits for cohorts whose faintest stars have $H \sim 12.8$ from 3 visits to 6 visits. This change ensures that all stars in these fields reach $S/N > 100$.

Implementation of the above action items required a net increase in the total number of visits assigned to the Bulge Program from 264 to 347 visits (a 31% increase).

To find this time, we elected to cancel the 25 Main Survey visits allocated to the Bulge RR Lyrae (RRL) Program described in Z17 (their Section 4.9). At the time that the Bulge Program was redesigned, a Contributed Program with the same goals (Section 5.6) had already completed a number of visits that far exceeded the 25 visits initially scheduled as part of the original APOGEE-2S targeting plan. Since the Contributed Program data become part of the overall APOGEE-2 data set, the Science Requirement goal for the Main Survey RRL program (~ 4000 stars) had formally been met (albeit not through the route intended), whereas, at the time, the “main red star” sample from the Bulge Program was not meeting its Science Requirement.

Still, 58 more visits had to be found to complete the new observation plan for the Bulge Program. At that point in the survey (2018 October), based on evidence for a growing APOGEE-2S observational efficiency that would deliver a final mean value that exceeded the estimate used in the design of the original survey (as discussed in Section 4.1), we found that the remaining 58 visits would be made up through faster completion of plates overall.

4.2.3. Summary of Bulge Modifications

Table 5 provides a summary of the most relevant information about the intended and actual Bulge Programs, in which we can see that even though the total number of bulge targets has decreased from the original plan by $\sim 19\%$ (6206 stars), the stars “lost” in the modified plan are the brightest, with $H < 11.0$; typically, stars brighter than $H \sim 11$ are more likely to be disk stars in the foreground to the bulge. The new plan significantly increases the number of stars in the magnitude

⁵² For context, the ASPCAP pipeline automatically flags anything with $S/N < 70$ with SN_WARN or bit 11 of ASPCAPFLAG (see Table 11 of Holtzman et al. 2015).

Table 5
APOGEE-2S Galactic Bulge Observing Plans

| Plan | Stars | Visits | Fields | “Short” Cohort | | “Medium” Cohort | | “Long” Cohort | |
|----------------|--------|--------|--------|------------------|------------------|-------------------------|------------------|-------------------------|------------------|
| | | | | $H < 11.0$ Stars | | $11.0 < H < 12.2$ Stars | | $12.2 < H < 12.8$ Stars | |
| | | | | S/N > 100 | $80 < S/N < 100$ | S/N > 100 | $80 < S/N < 100$ | S/N > 100 | $80 < S/N < 100$ |
| Original | 33,374 | 264 | 61 | 22,751 | 0 | 10,223 | 0 | 400 | 0 |
| New | 27,168 | 347 | 56 | 10,355 | 0 | 6525 | 3732 | 6253 | 303 |
| Percent Change | -19% | +31% | -9% | -55% | 0% | -37% | | +1463% | |

range $12.2 < H < 12.8$, which were practically nonexistent in the original plan, and the overall sky coverage of the new plan (Figure 3(b)) is almost equal to the one of the original plan (Figure 3(a)). It is also worth mentioning that even though the new plan will produce $\sim 15\%$ of stars observed in the Bulge Program with $S/N < 100$ per pixel, these stars will obtain, at a minimum, $S/N \sim 80$ per pixel, which does not represent a considerable cost to our science goals given current pipeline performance (Majewski et al. 2017; Jönsson et al. 2020).

4.3. Galactic Halo and Stellar Streams

The observing scheme for the Galactic halo and halo substructure in APOGEE-2 (both APOGEE-2N and APOGEE-2S) changed significantly from that presented in Z17. The original Halo Program was a uniform grid of pointings out of the Galactic plane, covering a range in $|b|$ from 30 to 75 degrees. While visits were set aside to sample streams in APOGEE-2N, no stellar stream observations were planned for APOGEE-2S, with the exception of a single field targeting the Sagittarius stellar stream (field name SRGT-2).

In APOGEE-2S, only two of the original halo grid fields, 280+45 and 320+45, were designed, each with 24 visits planned. The targets for these halo fields were selected using a color criterion of $(J - K_s)_0 > 0.3$ (dereddened color and employing the W+D giant method, Section 3.3.1) and no other targeting criterion. All of the other fields from the Halo Program, however, were designed using a new targeting strategy created to maximize the number of halo or stream candidates that could be observed with the LST visits available.

Then, the final APOGEE-2S Halo Program totals 41 fields and 258 visits: 48 visits split between the original 280+45 and 320+45 dedicated halo fields, 78 visits divided among the 13 new dedicated halo fields, 12 visits in the original dedicated stream field SGRT-2, and 120 visits split between the 25 new dedicated stream fields. The specific targeting priorities for each of these programs and their specific fields are given in the next subsections.

Dedicated halo fields have PROGRAMNAME tag value “halo”⁵³ and their field names were assigned based on their Galactic coordinates like all disk and bulge fields. For the dedicated stream fields, Sgr stream fields have PROGRAMNAME “sgr_tidal,” and other stream fields have PROGRAMNAME “stream_halo” or “stream_disk,” depending on the Galactic coordinates, and the field names for this program indicate the stellar stream being targeted. Even though the 15 dedicated halo fields and the 26 dedicated stream fields are both part of the APOGEE-2S Halo Program, we show their statistics in Table 4 and their spatial distribution in Figure 2 as separate cases to provide a higher level of detail for the reader.

⁵³ There is one exception for the field 066-79 that has PROGRAMNAME “halo2_stream” due to an error.

4.3.1. More Efficient Halo Targeting

In this section we explain how halo targets were selected for the fields in our Halo Program (while the selection of stream targets in these fields is explained in 4.3.2). An analysis of the data from APOGEE-2N halo observations suggested that the target selection was not observing enough stars at large line-of-sight distances to place them securely in the outer halo. This process and resulting changes are described in our companion paper on APOGEE-2N targeting (R. Beaton et al., submitted; AAS29028), but we summarize the key results here.

Prior to the Bright Time Extension (BTX), the Halo Program for APOGEE-2N relied on “deep” and “narrow-area” targeting using on the Washington + DDO51 photometry technique to identify likely giant stars from the dwarf star foreground (see Z13, Z17). While this strategy worked at $\sim 80\%$ efficiency to identify giants, the method was not particularly effective at identifying stars whose distances placed them securely in the outer halo; specific heliocentric distance limits were made in the APOGEE-2 Science Requirements Document for a certain number of halo stars to be surveyed at >15 kpc and >25 kpc, whereas the actual yields were around 3 times smaller than anticipated for survey goals (R. Beaton et al. submitted; AAS29028). By studying the proper motions of distant stars identified in APOGEE-1 and APOGEE-2N, it was found that proper motions could be used to remove the vast majority of the foreground dwarf contamination, which, in turn, greatly increased the likelihood of targeting a rare distant giant in a given field. As shown in R. Beaton et al. (submitted; AAS29028), the distant star yields using this procedure were between 2 and 3 times more effective than the original selection procedure. Because the APOGEE-2S halo targeting had not yet been fully implemented when the investigations described in R. Beaton et al. (submitted; AAS29028) were concluded, it was possible to incorporate the results of that investigation en masse for the APOGEE-2S Halo Program.

To maximize the number of halo stars in our APOGEE-2S Halo Program, we selected targets using the following priority ranking:

1. The highest halo candidate/member priority targets were selected from the SkyMapper survey (Keller et al. 2007). Casagrande et al. (2019) used SkyMapper (*uvgriz*) and 2MASS (*JHK_s*) photometry to produce $T_{\text{eff,phot}}$ estimates at a precision of ~ 100 K, metallicity estimates at 0.2 dex precision (for $[\text{Fe}/\text{H}] > -2$), and a reliable dwarf/giant separation. Using these data,⁵⁴ halo candidates were identified using the following criteria: $[\text{Fe}/\text{H}]_{\text{phot}} < -0.9$ and $3200 \text{ K} < T_{\text{eff,phot}} < 5500 \text{ K}$. Stars targeted using these photometric stellar parameters have bit 20 set in APOGEE2_TARGET2. These targets were included in all

⁵⁴ The catalog is available: <https://github.com/casaluca/SkyMapper>.

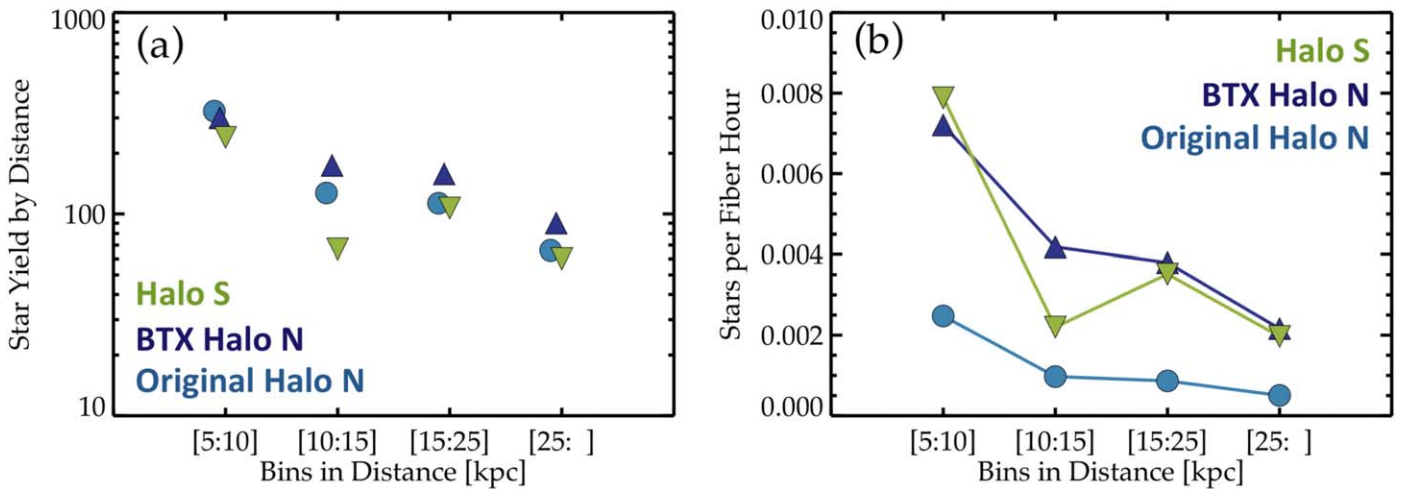


Figure 4. Comparison of the targeting efficiency for giants in Halo Programs. We compare the original halo targeting from APOGEE-2N that relied on Washington + DDO51 (“Original Halo N;” blue circles), the BTX APOGEE-2N targeting (“BTX Halo N;” purple up-pointing triangles), and the APOGEE-2S halo targeting (“Halo S;” green down-pointing triangles). For these figures, we only consider those stars that have measured stellar parameters ($\log g$ and T_{eff}) and we utilize spectrophotometric distances following the analysis described in Rojas-Arriagada et al. (2020, and references therein). (a) Number of stars in different distance bins. (b) Overall efficiency at identifying distant halo stars normalized by the total fiber hours in the program. The total fiber hours are computed by summing the number of visits that contribute to the final spectrum used for ASPCAP analyses for all of the targets in the program (NVISITS).

of the fields from our Halo Program except the two original dedicated halo fields 280+45 and 320+45.

- Then, we selected proper-motion candidates taken from the Gaia DR2 (Gaia Collaboration et al. 2018). The criteria for selecting these stars were $\mu < 5 \text{ mas yr}^{-1}$ and $\sigma_{\mu}/\mu < 0.1$ for all of the 13 new dedicated halo fields, and $< 5 \text{ mas yr}^{-1}$ and $\sigma_{\mu} < 0.2$ for the 18 new sgr_tidal stream dedicated fields. For the 15 fields sgr_tidal4 to sgr_tidal18 a magnitude limit of $H < 13.3$ was used for selecting these stars, while a magnitude limit of $H < 12.8$ was used for all other fields, which is standard for 6 visits fields (see Table 2). Stars selected using these proper-motion restrictions have bit 21 set in APOGEE2_TARGET2 flag.
- Then, for all APOGEE-2S Halo Program fields containing W + D photometry we incorporated W + D photometric giant candidates (see Section 3.3.1), and these targets have bit 7 set in APOGEE2_TARGET1.
- Finally, all APOGEE-2S Halo Program fields that still have remaining unassigned fibers are back-filled with stars from the “main red star” sample following the magnitude and color ranges appropriate for the number of visits, as given in Tables 2 and 3, respectively.

In Figure 4, we show the efficiency of the different halo targeting strategies used throughout APOGEE-2. These methods are: (1) the original method used for APOGEE-2N based on W + D photometry for giant-dwarf pre-classification (labeled “Original Halo N”), (2) the method used in the APOGEE-2N BTX based on HSOY proper-motion selection (Altmann et al. 2017) and SEGUE-confirmed distant K giants (labeled “BTX Halo N”; Xue et al. 2014), and (3) the modified APOGEE-2S halo selection described here, based on SkyMapper data and proper-motion information (labeled “Halo S”).

The left panel of Figure 4 shows the number of stars from each Halo Program obtained within broad distance bins. Overall, the total number of stars in each distance bin is more or less consistent between the three targeting methods, but to compare how successful each method was we also need to consider the observing time invested in each Halo Program.

Thus, to calculate the efficiency of each method, we normalized the number of stars observed within each distance bin by the total number of “fiber hours” from each program, where a *fiber hour* is one visit for a single fiber from a plate, and a single plate visit has a total of 265 fiber hours dedicated to stars. This means that a single star from the Halo Program observed N times adds N fiber hours to total of the Halo Program, and for plates dedicating fibers to more than one program (e.g., APOGEE-2N plates with both Halo and ancillary program stars) only the fibers dedicated to the Halo Program would count toward the total sum of fiber hours for the Halo.

The right panel of Figure 4 shows the number of Halo Program stars obtained per distance bin divided by the total number of fiber hours associated with each Halo Program. The APOGEE-2S strategy is about 3 times more effective than the original APOGEE-2N halo strategy in terms of observing distant halo stars for all distance bins. This demonstrates that altering the targeting strategy for APOGEE-2S has resulted in a much more efficient method for pre-selecting distant halo stars than was originally used in APOGEE-2. That said, the APOGEE-2S and APOGEE-2N BTX halo targeting strategies show similar efficiencies, as displayed in Figure 4(b). Achieving this for APOGEE-2S is remarkable given that APOGEE-2N includes known halo members from SEGUE that were not available for APOGEE-2S, and the plates in APOGEE-2N have a larger FOV that enable mapping larger region of the sky in a single visit.

4.3.2. Targeting Stellar Streams

To increase the number of halo stars in APOGEE-2S while simultaneously sampling halo substructure, we added 25 dedicated fields, whose locations were placed on the footprints of known stellar streams. This represents one of the most important changes to our observing plan, considering that originally the Halo Program only contained one dedicated stream field called SGRT-2. The 26 dedicated stream fields were designed targeting three streams in the Southern Hemisphere, and were split in the following way:

1. Nineteen fields placed on the Sagittarius (Sgr) stream, consisting of field SGRT-2, fields Sgr_tidal1 to Sgr_tidal3, and fields sgr_tidal4 to sgr_tidal18. All of these fields have PROGRAMNAME “sgr_tidal.”
2. Six fields (JHelum1 to JHelum6) placed on the Jhelum stream. All of these fields have PROGRAMNAME “stream_halo.”
3. One field placed on the Orphan stream (Orphan1), with PROGRAMNAME “stream_disk.”

Besides these 26 dedicated stream fields, Sgr stream targets were added to 8 dedicated halo fields (032-62, 037-43, 060-72, 066-79, 120-85, 137-71, 173-61, and 179-57), and Orphan stream targets were added to the dedicated halo field 339-44. This means that our Halo Program includes a total of 27 fields targeting Sgr stream targets, 6 fields targeting Jhelum stream targets, and 2 fields targeting Orphan stream targets. Throughout this subsection we are going to explain how we selected targets from these 3 streams in all of these fields.

Sagittarius Stream Selection: The original dedicated stream field SGRT-2 selected targets from the Sgr stream based on W + D dwarf/giant classification, and the location of the stars in a $([J - K_s]_0, H)$ color–magnitude diagram (CMD; see Z17 for more details). In the new APOGEE-2S Halo Program, we included Sgr stream targets in 18 new dedicated stream fields, and 8 new halo dedicated halo fields, by using the candidate stars presented in Hayes et al. (2018a) as our parent sample.

To describe the regions observed in this stream, we use the heliocentric Sgr spherical coordinate system presented in Majewski et al. (2003). In this system, the equator is defined by the Sgr debris midplane and corresponds to a pole with Galactic coordinates $(\ell, b) = (273.8, -13.5)$. Then, Sgr latitudes, $|B_\odot|$, are defined as the angular distance to the Sgr debris equator as viewed from the Sun, and Sgr longitudes, Λ , are defined to increase in the direction of trailing Sgr debris, with $\Lambda = 0$ defined as the longitude of Sgr center from the King profile fitting results of Majewski et al. (2003).

Hayes et al. (2018a) identified candidate Sgr stream red giants in the magnitude range of $10 < H < 13.5$ lying at Sgr stream latitudes of $|B_\odot| \lesssim 20^\circ$ along $\sim 90^\circ$ of the trailing arm of the Sgr stream. Because the Sgr stream is kinematically colder than the rest of the local halo, these candidates could be selected confidently based on their proper motions, particularly in having small, halo-like proper motions that are oriented in the direction of motion of the Sgr stream (see Hayes et al. 2018a). The locations for the 18 new stream dedicated Sgr tidal fields (called Sgr_tidal1 to Sgr_tidal3 and sgr_tidal4 to sgr_tidal18) were selected to maximize the number of Sgr stream candidates from this sample and the spatial coverage along the stream. The 8 new dedicated halo fields also included Sgr stream candidates from the Sgr sample, but the field location was chosen to maximize halo targets (see Section 4.3.1) over stream targets. As a result of these changes, the APOGEE-2 coverage of the Sgr stream goes more or less homogeneously from $\Lambda = 35^\circ$ to $\Lambda = 110^\circ$ at Sgr stream latitudes of $|B_\odot| \lesssim 10^\circ$ (ℓ from 10° to 175° and b from -48° to 82°).

Jhelum Stellar Stream Selection: Six dedicated stream fields were designed to target the Jhelum stream (Bonaca et al. 2019; Shipp et al. 2018), with FIELD of “JHelum1” through “JHelum6”. The fields were selected by tracing the stream using Gaia DR2 photometry and astrometry. Candidates were selected as high-probability members of the stream based on their proximity (in sky position) to the stream track defined by

Bonaca et al. (2019), and by modeling the (solar motion corrected) proper-motion distribution along the stream.

In detail, following the method used in Price-Whelan & Bonaca (2018), we construct a mixture model for the full proper-motion distribution in this part of the sky. A Gaussian mixture model (GMM) representation of the “background” proper-motion distribution was first constructed by fitting a GMM to the proper-motion distribution of stars in a sky track offset by two degrees north and south (in a Jhelum stream aligned coordinate system; Bonaca et al. 2019). At locations along the Jhelum stream track, we then fit a mixture model containing the GMM background model as one component, and a single Gaussian with a varied mean and variance as the “stream” component. We also fit for the mixture weight, which defines the relative contribution of the stream and background components to the total proper-motion distribution.

This model is then used to assign membership probabilities to stars in the vicinity of the Jhelum stream. Stars were selected with $>50\%$ membership probability that also lie within 0.25 mag of the red giant branch for a metal-poor ($[Fe/H] = -2$) isochrone (from the MIST stellar isochrone library; Dotter 2016; Choi et al. 2016). By this means, a total of seven candidate stars from the Jhelum stream were selected. The dedicated publication on the Jhelum stream provides some additional details (Sheffield et al. 2021).

Orphan Stellar Stream Selection: Orphan stream (Belokurov et al. 2006; Koposov et al. 2019) targets were included in the dedicated halo field 339-44 and the dedicated stream field Orphan1. To select candidate Orphan stream members, we use the sample of RR Lyrae type Orphan stream stars from Koposov et al. (2019) to fit polynomial trends in sky position and the two proper-motion components (all in the Orphan stream coordinate system defined in Koposov et al. 2019). We then select all sources with Gaia DR2 astrometry and 2MASS photometry in a 70° by 10° region around the extension of the Orphan stream into the Southern Hemisphere. We use the polynomial tracks of the stream (determined from the RR Lyrae star members) combined with a color–magnitude selection using a metal-poor ($[Fe/H] = -2$) isochrone (from the MIST stellar isochrone library; Dotter 2016; Choi et al. 2016) to select candidate red giant branch star members of the stream. A dedicated publication on the Orphan stream will provide additional details (K. Hawkins et al. 2021, in preparation).

All stars targeted as stellar stream candidates have bit 18 set in APOGEE2_TARGET1. The remaining targets in each field were selected following the halo targeting strategy discussed in Section 4.3.1.

4.4. Dwarf Spheroidals: Fornax

Because of improvements in survey efficiency and the allocation of extra nights to APOGEE-2S it was possible to expand the coverage of the survey and add an additional dwarf galaxy to APOGEE’s sample, the Fornax dSph galaxy (Shapley 1938). As for all of the other dSphs in APOGEE-2S, Fornax was planned to be observed with a single cohort of targets for 24 visits. Stars for this field were selected using a combination of spectroscopic, photometric, and proper-motion information that we now describe.

At highest priority, we targeted four of the five confirmed Fornax globular clusters (Hodge 1961), three of which were targeted as integrated light observations (Fornax 3, 4, and 5), while for the fourth cluster (Fornax 2) we specifically targeted

the brightest star. These integrated light observations complement programs in APOGEE-1 for M 31 globular clusters (Sakari et al. 2016, Z13) and in APOGEE-2N for M 33 clusters (a description is given in R. Beaton et al. submitted; AAS29028).

At second priority we targeted individual Fornax member stars identified by prior radial velocity and chemical abundance analyses using FLAMES on the Very Large Telescope from Letarte et al. (2010) and Lemasle et al. (2014). Additional radial velocity members from the wide-area survey with Magellan+M2FS by Walker et al. (2009) were added at third priority.

Because many spectroscopic studies have small footprints compared to the APOGEE-2S FOV, additional candidate members were selected by combining ground-based photometry with Gaia DR2 proper motions. The photometry came from two sources: (1) optical CFHT photometry from Muñoz et al. (2018; highest priority) and (2) NIR photometry from 2MASS (Skrutskie et al. 2006). Lastly, we included photometric candidates from the NIR study of Gullieuszik et al. (2007). In all categories, stars below the tip of the red giant branch (i.e., with magnitudes $14.7 < H < 15.2$) were selected ahead of stars with asymptotic giant branch (AGB) like magnitudes above the tip of the red giant branch (i.e., $H < 14.7$).

4.5. Magellanic Clouds

Targeting of the Magellanic System—the Large and Small Magellanic Clouds (LMC, SMC) and the substructure in their vicinity—formed a major component of the APOGEE-2S program; a summary is given in Z17 with additional details and the first results of the program given in Nidever et al. (2020). For reference, the Magellanic Clouds program pulled targets from a variety of targeting classes to cover a wide range of luminous stellar evolutionary states, while also building a sample of red giants, which could be reliably analyzed by APOGEE and compared to Milky Way red giant samples. For context, the targeting classes for general LMC and SMC targeting are as follows, in order of priority:

1. Supergiants following Neugent et al. (2012) and Bonanos et al. (2009; limited to ≤ 20 per plate),
2. Hot main-sequence stars (limited to ≤ 20 per plate),
3. Olsen et al. (2011) retrograde stars (limited to ≤ 20 per plate),
4. Post-AGB stars from Kamath et al. (2014, 2015; limited to ≤ 10 per plate),
5. Red giant branch (RGB) stars with high-resolution public spectroscopy (limited to ≤ 10 per plate),
6. AGB Carbon-rich stars following Nikolaev & Weinberg (2000; limited to ≤ 20 per plate),
7. AGB Oxygen-rich stars (limited to ≤ 20 per plate),
8. RGB stars (≥ 130 per plate).

All designs belonging to Magellanic Cloud fields in the Main Survey have a PROGRAMNAME tag value of “magclouds.”

The Magellanic Clouds Program was augmented in three ways: (1) expanded LMC and SMC spatial coverage, (2) an optical cross-calibration field, and (3) the inclusion of a Contributed Program in the Main Survey.

Expanded Spatial Coverage: The COVID-19 pandemic closed operations of APOGEE-2S from March 2020 to October 2020 and after reopening, the APOGEE-2S observations

spanned an ideal time of the year to focus on the Magellanic Clouds. A total of 23 new fields were added, placing five 12 visit fields in the SMC (named SMC8–12) and the remaining 18 9 visit fields placed throughout the LMC (named LMC18–35). This increases the SMC coverage by 70% and the LMC coverage by 106%. The target selection for these fields is identical to that summarized above (see also Nidever et al. 2020, Z17).

Optical Calibration: The APOGEE-2S Magellanic Cloud program is one of the largest spectroscopic surveys of the Magellanic System, but there was very little overlap with prior studies in the optical to which the APOGEE near-infrared based measurements could be directly compared. To rectify this, we added an APOGEE field that overlaps with the study of Van der Swaelmen et al. (2013) that measured stellar parameters and elemental abundances from optical spectroscopy. While the APOGEE-2S targeting primarily focused on the most luminous stars in the LMC, Van der Swaelmen et al. observed stars lower on the giant branch. The purpose of this field is to characterize any differences between the target selection of APOGEE-2 and Van der Swaelmen et al. (2013; e.g., upper versus mid-giant branch and results derived from infrared spectra). Some early evaluations of these differences are given in Nidever et al. (2020).

This field is named “LMC_VdS” with a field center at $(\ell, b) = (283, -34)$ and was observed using a single cohort in a 24 visit design. Using a plate radius of $1^\circ 0$, 67 targets from Van der Swaelmen et al. (2013) were prioritized to a limiting magnitude of $H = 14.5$ mag, with three stars rejected due to fiber collisions. The targets from Van der Swaelmen et al. (2013) have targeting bit 22 set in APOGEE2_TARGET1 because they are confirmed members. The remaining fibers in this field were selected following the standard LMC target selection. The corresponding depth for both targeting schemes is $H = 14.5$ and this is fainter than the magnitude limit needed to reach our nominal S/N = 100 goal in a 24 visit field (see Table 2).

LMC Substructure: A Contributed Program (see Section 5.16) targeted the LMC substructure and these observations were coordinated with the Magellanic Clouds Working Group. As part of the COVID-19 extension, these were folded into Main Survey and each plate was allocated additional visits to reach the survey S/N goal at 9 visits. No changes were made to the targeting bits or PROGRAMNAME to reflect this change. For details on this program see Section 5 for the general implementation of Contributed Programs and Section 5.16 specifically.

In all survey fields focused on the Magellanic Clouds, the following targeting bits are used. Confirmed Magellanic Cloud members have targeting bit 22 set in APOGEE2_TARGET1. Potential Magellanic Cloud stars, with candidates typically identified using photometric criteria, have targeting bit 23 set in APOGEE2_TARGET1. The PROGRAMNAME for this program is “magclouds.”

4.6. Open Clusters

Open clusters are important tools to study the chemical patterns and evolution of the disk, and targeting such objects has been a major component of APOGEE-1 and APOGEE-2. In particular, the Open Cluster Chemical Abundance and Mapping (OCCAM) Survey has worked to ensure that as many open clusters as possible are included in the APOGEE footprint (e.g.,

Frinchaboy et al. 2013; Donor et al. 2018, 2020). In DR16, Donor et al. (2020) found 128 clusters had some observations, with 71 clusters having sufficiently many members to be used to study chemical gradients in the disk.

Targeting for the open clusters proceeds in a series of steps that are explained in detail in the OCCAM papers (Frinchaboy et al. 2013; Donor et al. 2018, 2020) as well as in Z13 and Z17. First, the cluster mean proper motion is determined using a kernel convolution method. Stars closer to the cluster average proper-motion value are given higher priority and, where available, spectroscopic and/or kinematic member stars from previous studies are targeted. Finally, photometry is used to remove clear nonmembers from the color–magnitude diagram. Stars selected as potential open cluster members have the targeting bit 9 in APOGEE2_TARGET1 set.

Additions to the Open Cluster Sample: The goal in supplementing the Open Cluster sample was specifically to target distant clusters in both the inner and outer Galaxy to improve measurements of the Galactic abundance gradient (e.g., Frinchaboy et al. 2013; Donor et al. 2018, 2020). Additionally, clusters were included to help expand our cluster-based calibration efforts for both the metal-rich and relatively metal-poor extremes that can be probed by open clusters (see, e.g., Holtzman et al. 2018). We added six open clusters amounting to 20 visits; these clusters are Berkeley 75, Berkeley 81, NGC 5999, NGC 6583, NGC 6603, and Tombaugh 2.

Main Sequence Calibrators in M 67: The COVID-19 extension opened up some time during which the open cluster M 67 was observable. APOGEE-2N designed a field dedicated to observing down the main sequence of M 67 to build a calibration sample of M dwarfs (see R. Beaton et al. submitted; AAS29028). However, this 36 visit field could not be completed in the COVID-19 modified schedule for APOGEE-2N, and only 10 visits were performed in this field. Because this important calibration field could not be finished in APOGEE-2N, and time was available with the COVID-19 extension to APOGEE-2S, the decision was made to re-design this northern field for southern observation. While this required changing the targets slightly from the original design, which is described in R. Beaton et al. (submitted; AAS29028), due to the difference in plate scale and FOV between APOGEE-2N and -2S, the target selection and design follows the description given there, though we note that the targets are not one-to-one identical.

4.7. K2

APOGEE-2N initiated a large-scale campaign to obtain complementary APOGEE spectra in the K2 campaigns (described in R. Beaton et al. submitted; AAS29028). The full program was difficult to accommodate fully in APOGEE-2N and, with the goal of providing the most complete possible scientific data set leveraging K2, we transferred 87 1 visit fields from six different K2 campaigns to the APOGEE-2S field plan. At the time of this decision, comparisons of the relative performance of the ASPCAP pipeline on targets observed both with APOGEE-2N and APOGEE-2S suggested that splitting the program would not cause a bias in the K2 scientific results (a full discussion is given in Jönsson et al. 2020). The fields transferred to APOGEE-2S plan correspond to Campaigns C8, C10, C14, C15, and C17, and half of the fields from C6. We note that the differences between the FOV and plate scale mean that the plates for APOGEE-2N and APOGEE-2S are not

identical, and this should be taken into account if data from both telescopes are combined.

We briefly summarize the targeting here, noting that a more involved discussion is given in R. Beaton et al. (submitted; AAS29028). The targeting made use of knowing which stars were already targeted by HERMES (Sheinis et al. 2015; Sheinis 2016) using the setup used in the GALAH survey (Wittenmyer et al. 2018; Sharma et al. 2019). In addition, asteroseismic oscillator identification following the data processing and analysis of Hon et al. (2019), but applied to K2 data, was performed before targeting; these asteroseismic results have been published in Zinn et al. (2020) for three K2 campaigns. From all stars with K2 data, we first remove stars with existing APOGEE observations (APOGEE-1 or APOGEE-2). From here the targets were prioritized as follows:

1. Known planet hosts (APOGEE2_TARGET2 bit 11),
2. Stars with a confirmed oscillation or granulation signal (APOGEE2_TARGET1 bit 30),
3. Red giants targeted by the K2 Galactic Archaeology Program (GAP; Stello et al. 2017, APOGEE2_TARGET2 bit 0) and *not* observed with HERMES,
4. GAP targets observed by HERMES (see Wittenmyer et al. 2018; Sharma et al. 2019, APOGEE2_TARGET2 bit 17),
5. M dwarfs in the unbiased sample from the APOGEE-2N ancillary program (APOGEE2_TARGET3 bit 28),
6. Stars meeting the criteria for the “main red star” sample (APOGEE2_TARGET1 bit 14).

While the target selection was prioritized following this scheme, an individual target could be present in multiple target categories. Field centers were optimized to reach the most targets weighted by priority.

All APOGEE-2N K2 observations will have the PROGRAMNAME “k2_btx” and field names like “K2_C#_III ± bb_btx”, where C# indicates the K2 campaign and III ± bb indicates the Galactic coordinates for the field center. For APOGEE-2S K2 observations the PROGRAMNAME is “k2” and the field names have format “K2_C#_III ± bb.” All targets in K2 fields have APOGEE2_TARGET3 bit 6 set, as well as specific flags for the subtargeting category as detailed above.

4.8. Globular Clusters

The original targeting of globular clusters in APOGEE-2S is described generally in Z17. While there were no changes to the globular cluster program during the main survey of APOGEE-2S, the COVID-19 extension allowed for the expansion of observations on four globular clusters: NGC 1851, NGC 2808, M 79, and ω Centauri (ω Cen), and the design of a new globular cluster field, NGC 2298, in total summing to 30 new visits, with six per cluster. For NGC 1851, NGC 2808, and M 79, new designs were created to target known members from Sollima (2020) that are brighter than $H = 12.8$ mag. A new field (FIELD of N2298) was made to target the globular cluster NGC 2298, and similarly, targets for this cluster were taken from Sollima (2020) with the same magnitude limit. The member stars from these five clusters are flagged with APOGEE2_TARGET2 bit 10.

4.8.1. Omega Centauri

In the original targeting of ω Cen, the acquisition camera, with its 5.5' occlusion radius, was placed near the center of the cluster, blocking the core of the cluster from observation. This notably leaves a significant gap in the APOGEE-2 spatial coverage of ω Cen, with the central 5.5' of Omega Centauri containing no APOGEE targets due to the central obscuration (see Figure 1). In addition, since the design of the original ω Cen field, Ibata et al. (2019) used Gaia DR2 (Gaia Collaboration et al. 2018) observations to reveal a thin tidal stream coming off of ω Cen. This too motivated observing more of ω Cen.

With some of the time made available in the COVID-19 extension of APOGEE-2S, it was decided to allocate some of the available time to better cover ω Cen and fill in this spatial coverage gap (by moving the field center, and therefore the location of the acquisition camera to a different position on the sky), albeit not to the same depth as originally designed. Instead of the 24 visits assigned to the original ω Cen field—which were split into two sets of long cohorts that received 12 visits each, with short and medium cohorts receiving 3 and 6 visits, respectively—the new ω Cen field (FIELD named “Omegacen2”) was designed to have 6 visits, which were split into two sets of medium cohorts that received 3 visits each, with short cohorts receiving 1 visit each. The minimum magnitude for this field was lowered to $H = 12.8$ for special targets, instead of the nominal $H = 12.2$ for a 3 visit faint cohort, and $S/N \sim 70$ was deemed sufficient.

The target selection for this new field, first, prioritized observing stars with high-resolution optical spectra from Johnson et al. (2020), followed by proper-motion identified ω Cen members from van Leeuwen et al. (2000), and finally ω Cen stream candidates were prioritized last; however, because of their low sky density and distance from the center of the cluster, all of the identified candidates were included. Unfortunately, the identification of the ω Cen stream by Ibata et al. (2019) was performed with dwarf stars, which were too faint for APOGEE-2S to observe at the distance of ω Cen. So, Stream candidate giants were identified by consolidating stream candidates from Anguiano et al. (2015), Fernández-Trincado et al. (2015), and stars observed by the STREGA survey outside of ω Cen’s tidal radius and along ω Cen’s sequence in the g_0 versus $(g - i)_0$ color-magnitude diagram (STRUCTURE and Evolution of the GALaxy with the VST; Marconi et al. 2014). These latter stars were also required to have Gaia DR2 proper motions within 1.6 mas yr^{-1} of the bulk proper motion of ω Cen $(\mu_\alpha \cos(\delta), \mu_\delta) = (3.24, -6.73)$ from Baumgardt et al. (2019). ω Cen members with optical spectra or identified from their proper motions have been flagged with APOGEE2_TARGET2 bit 10 and the ω Cen stream candidates have been flagged with APOGEE2_TARGET1 bit 19.

5. Contributed Programs

Roughly 23% of the observing time of the APOGEE-S spectrograph was used for programs that are independent of the main survey observing plan and thereby do not follow the main survey targeting strategies. Such programs are allocated either through the Chilean Time Allocation Committee (CNTAC) or by the Observatories of the Carnegie Institution of Science TAC (CIS) and are both scheduled “classically” for specific night(s) and observed “classically” (in the sense that time lost

on a given night is only recovered through a subsequent TAC allocation). From 2016 to 2020, 104 nights were used for Contributed Programs following the ratio of Main Survey versus Contributed Program nights of approximately 3:1 per annum.

The targeting scheme of each of these programs is entirely decided by its Principal Investigator (PI) via the submission of special targets; this includes what is observed, for how long and, if applicable, at what cadence. The APOGEE-2S team only applies some basic restrictions to the target lists to ensure that the plates can be plugged and are observable during the night(s) assigned to the program.

The PI(s) of each project may choose whether the observed data would be included in the SDSS Data Releases, known as “Contributed Programs,” or if the data would remain external to the survey, known as “External Programs.” For Contributed Programs, while the data are collected according to the specifications of the TAC and the PIs, the spectroscopic data, itself, are treated identically to those of the main survey. More specifically, the data are processed with the existing APOGEE data processing pipelines, are made into the same data products, and are made available to the collaboration in the same way. For the duration of APOGEE-2S, all of the PIs chose for their observations to be executed as “Contributed Programs.”

Table 6 provides the main observational aspects of the 19 Contributed Programs, including the nominal depth calculated based on the maximum visits received per star. Figure 5 provides the sky distribution of Contributed Programs. Each field is color coded by the planned field depth (recall, 1 visit is roughly 1 hour of on-sky integration) to provide a sense of the targeting strategy. The two insets in Figure 5 zoom in on particularly densely targeted regions of the sky.

Field naming conventions from the main survey were adopted for these programs, but the fields from Contributed Programs have “-C” and “-O” appended to their name, for CNTAC and CIS programs, respectively. Fields from the TESS CIS program specifically (TeskeVanSaders_18a; Section 5.8) have a further “_TESS” appended at the end of their names. Targets included in these observations have bit 24 and 25 set in APOGEE2_TARGET2 flag for CIS and CNTAC programs, respectively.

Because the targets are not selected following standard APOGEE-2 procedures, the programs are not identifiable using targeting bitmasks. Each program is, instead, identified by its “program name” in the PROGRAMNAME tag (given in Table 6). The program name is typically constructed as the last name of the PI followed by the first semester it was allocated; because of the classical-style implementation of these programs, many programs spanned multiple observing semesters.

In the sections that follow, we provide descriptions of the 19 individual Contributed Programs in regards to their observations and science goals, contact scientists, and the awarding time allocation committee. Just as for the survey descriptions, these correspond to the program as designed and do not reflect the level of completeness obtained by the program by number of fields, number of stars, or intended S/N .

5.1. Star-forming Region G305

Contact Information: J. Borissova (Universidad de Valparaíso).

Table 6
Summary of APOGEE-2S Contributed Programs

| Program Name | TAC | Program Name | Total Visits | Total Stars | Stars Observed | Average SNR | Depth H [mag] | Subsection | Contact |
|--------------------------------------|-------|--------------------------|--------------|-------------|----------------|-------------|-----------------|------------|---|
| Star-forming Region G305 | CNTAC | borissova_17a | 8 | 1000 | 250 | 71.4 | 12.2 | 5.1 | J. Borissova |
| Cool dwarfs in K2 fields | CIS | teske_17a | 43 | 10,750 | 7250 | 134.9 | 11.0 | 5.2 | J. Van Sadere |
| Upper Scorpius cluster | CIS | TeskeVanSadere_17b | | | | | | | |
| | | weinberg_17a | 98 | 21,750 | 5106 | 143.0 | 11.7 | 5.3 | A. Weinberger |
| | | weinberg2_17a | | | | | | | |
| Inner bulge and disk | CNTAC | zoccali_17a | 17 | 3750 | 1750 | 91.4 | 11.7 | 5.4 | M. Zoccali |
| | | zoccali_18b | | | | | | | |
| Metal-poor stars in the inner Galaxy | CIS | schlaufman_17a | 18 | 4500 | 3000 | 97.1 | 11.0 | 5.5 | K. Schlaufman |
| The structure of the Ancient MW | CIS | kollmeier_17a | 43 | 10,750 | 10,250 | 47.5 | 11.0 | 5.6 | J. Kollmeier |
| Low metallicity Cepheids | CIS | beaton_18a | 18 | 1500 | 1500 | 195.1 | 12.2 | 5.7 | R. Beaton |
| TESS/APOGEE survey | CIS | TeskeVanSadere_18a | 154 | 38,500 | 26,500 | 168.1 | 11.0 | 5.8 | J. Teske, J. Van Sadere and R. Beaton |
| Carina Star-forming Complexes | CNTAC | RomanLopes_18a | 5 | 750 | 750 | 175.3 | 12.2 | 5.9 | A. Roman-Lopes |
| Corona Australis protocluster | CNTAC | stutz_18a | 4 | 500 | 500 | 135.9 | 11.7 | 5.10 | A. Stutz |
| Bulge globular clusters | CNTAC | geisler_18a, geisler_19a | 57 | 5561 | 3217 | 106.9 | 12.8 | 5.11 | D. Geisler |
| | | geisler_18b, geisler_20a | | | | | | | |
| Massive Stars in the SMC and LMC | CIS | Drout_18b | 22 | 5250 | 3500 | 130.5 | 11.7 | 5.12 | M. Drout |
| Rosette Molecular Clouds | CNTAC | stutz_18b | 4 | 370 | 370 | 56.5 | 12.2 | 5.13 | A. Stutz |
| Carina Protocluster | CNTAC | stutz_19a | 6 | 750 | 500 | 66.3 | 11.7 | 5.14 | A. Stutz |
| OB Stars | CIS | kollmeier_19b | 42 | 2750 | 500 | 160.6 | 12.8 | 5.15 | J. Kollmeier A. Tkachenko |
| LMC substructures | CNTAC | monachesi_19b | 21 | 1500 | 1250 | 55.7 | 12.4 | 5.16 | A. Monachesi |
| Orion Nebula Cluster | CNTAC | stutz_20a | 7 | 1000 | 0 | 0.0 | 11.7 | 5.17 | A. Stutz |
| Carina Nebula Cluster | CNTAC | medina_20a | 7 | 750 | 0 | 0.0 | 12.2 | 5.18 | N. Medina |
| NGC6362 cluster | CNTAC | fernandez_20a | 2 | 500 | 0 | 0.0 | 11.0 | 5.19 | J. Fernández-Trincado |

Located within the Scutum-Crux arm of the Milky Way ($\ell = 305^\circ.4$, $b = 0^\circ.1$), with a projected diameter of 30 pc, the G305 star-forming complex is both relatively nearby (~ 3.8 kpc) and one of the most luminous H II regions in the Milky Way (Urquhart et al. 2014). The region contains several distinct sites and epochs of star formation, which permits the study of massive star formation, massive star evolution, and the impact of these processes on the surrounding environment. The morphology of the region and positions of star formation indicators suggests that interaction between the evolved massive stars and remnant, natal molecular material is taking place, resulting in ongoing star formation activity. Thus, G305 region is a perfect test-bed object, both for intermediate- and high-mass star formation.

The scientific aim of this project is to analyze the kinematics and metallicity of stars in G305 region. The project will combine the homogeneous, high-precision photometry and variability from VVV (Minniti et al. 2010), astrometry from Gaia DR2 (Gaia Collaboration et al. 2018), and radial velocity and metallicity measurements from APOGEE-2. With these data, the project will: (1) improve the census of both massive and intermediate-mass stars in the area; (2) measure the kinematics of different stellar groups (young stellar objects, OB, WR stars) and confirm/reject memberships of the stars to the clusters projected in the region; (3) outline the potential spatial substructures and measure the star formation histories to probe models of triggered versus passive star formation; and

(4) calculate the present-day star formation rate in the area using the method of direct counts of young stellar objects as compared with that of other star-forming regions in the Milky Way. Some results from these observations are published in Borissova et al. (2019). Observations from this project have PROGRAMNAME borissova_17a.

5.2. Cool Dwarfs in K2 fields

Contact Information: J. van Sadere (University of Hawaii) and J. Teske (Carnegie Institution For Science, Earth and Planets Laboratory).

The goal of this program is to collect APOGEE-2S spectra of bright, cool dwarf stars that are being monitored by the K2 ecliptic survey (Howell et al. 2014), including stars known to host planet candidates through the analysis of their light curves. These data will be used to measure stellar parameters and chemical abundances for low-mass stars in the K2 fields. The scientific goals are: (1) to determine rotation-based ages, (2) to constrain the age-metallicity relation, and (3) to look for a correlation between exoplanet architecture and host-star composition. In particular, M-dwarf spectra are of high value in the development of an analysis method for extracting reliable, detailed abundances of $T_{\text{eff}} < 4000$ K stars. This project aims at observing 34 fields from six K2 Campaigns: C1, C2, C3, C4, C7, and C8. Observations from this project have PROGRAMNAME teske_17a, or TeskeVanSadere_17b.

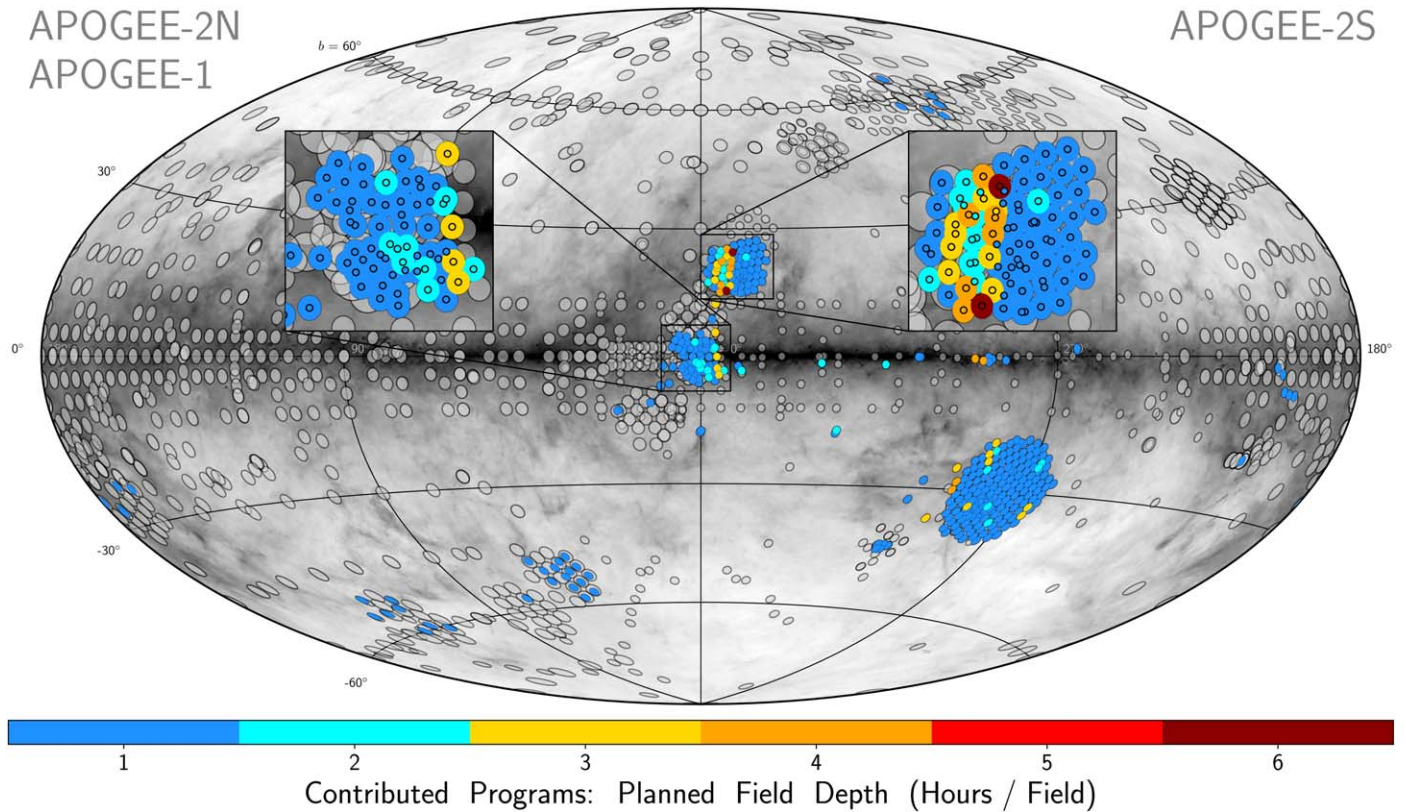


Figure 5. Sky distribution of APOGEE fields highlighting in color those from APOGEE-2S Contributed Programs. The color coding indicates the number of visits observed per field; gray symbols represent all other fields for context. The background image is the dust map from Schlegel et al. (1998). The inlays indicate the dense targeting in the Galactic center (left) and the Upper Scorpius star-forming region (right), where we have overlaid circles to indicate the unique plate centers. These fields represent $\sim 23\%$ of the APOGEE-2S observing program.

5.3. Upper Scorpius Cluster

Contact Information: A. Weinberger (Carnegie Institution For Science, Earth and Planets Laboratory).

This program aims to survey the young (~ 10 Myr old), Upper Scorpius cluster to measure the properties of a large, homogeneously targeted population of young stars. We primarily target cluster members that were included in K2 and for each star we intend to measure T_{eff} , $\log g$, and radial velocity.

The targets for this project come from three separate sources:

1. We included all targets fainter than $H = 7.5$ from three K2 guest observer programs during Campaign 2⁵⁵ that focused on Upper Sco. These are Program 2052 (PI Covey: *K2 Monitoring of Confirmed Members of Upper Sco and Rho Oph*), Program 2057 (PI Hillenbrand: *A K2 Study of Young Stars in Upper Scorpius*), and Program 2063 (PI Kraus: *Planets Around Likely Young Stars in Upper Sco and Rho Oph*). These account for 1309 targets.
2. We included all additional (16) Upper Sco targets that were part of a ground-based parallax survey (Donaldson et al. 2017); these were all fainter than $H = 7.5$.
3. We included additional Upper Sco targets that were part of the Spitzer surveys of Upper Sco looking for circumstellar disks and were fainter than $H = 7.5$ (78 targets; Carpenter et al. 2005, 2006a, 2006b, 2009).

Thus, there were 1403 sources included in our master target list. When constructing input lists for the APOGEE-S targeting software, we allowed targets in the vignettted ($0.8\text{--}0.95^\circ$ radii) region of the field.

Observations from this project have PROGRAMNAME of weinberg_17a, or weinberg2_17a.

5.4. Inner Bulge and Disk

Contact Information: M. Zoccali (Pontificia Universidad Católica-Instituto Milenio de Astrofísica).

The region called the “Nuclear Bulge” stands out from the main bulge due to several observed properties: (1) a much higher stellar density, with a clear break (Launhardt et al. 2002), (2) the presence of a dense interstellar medium (the Central Molecular Zone; Morris & Serabyn 1996), (3) ongoing star formation in scattered dense clouds, and (4) a stellar nuclear disk. The presence of a stellar nuclear bulge has been confirmed with APOGEE data (Schönrich et al. 2015), however many open questions remain regarding its formation and relationship to other bulge structures.

To sample this region with APOGEE, five fields were designed at the following Galactic coordinates (ℓ , b): $(-4, 0)$, $(-2, 0)$, $(0, 0)$, $(2, 0)$, and $(4, 0)$, respectively. Targets were selected from imaging from VISTA Variables in the Via Lactea (VVV; Minniti et al. 2010), but with point-spread function photometry derived by Rodrigo Contreras (private communication) with the method described in Contreras Ramos et al. (2017). Because the interstellar extinction toward the nuclear bulge is extremely large ($A_V > 20$) the observed red giant

⁵⁵ <https://keplerscience.arc.nasa.gov/k2-approved-programs.html#campaign-2>

branch has a very broad distribution in color. To define a target box in color–magnitude space that creates a uniform sampling of the stellar populations at different metallicities, an initial selection of stars with $2.4 < E(J - K_s) < 3$ was imposed, using the reddening maps from Gonzalez et al. (2018). In the central field, this color cut excluded stars within ± 0.3 of the Galactic plane, but permitted the CMD box with $H < 11.8$ to span the full RGB color range for the other four fields without imposing a significant color bias. If not designed out of the sample selection, a color bias could introduce a metallicity bias; we note that the color range is different for each of the fields.

The APOGEE observations will be used to derive the metallicity distribution function for these regions and it will be used to test if the nuclear disk is the central extension of the inner bulge, or if it is a distinct stellar component. Furthermore, an empirical metallicity distribution function will break the degeneracy in the derivation of the star formation history of this region by comparing the available deep NIR CMDs (Nogueras-Lara et al. 2019) with synthetic color–magnitude diagrams. Observations from this project have PROGRAMNAME of zoccali_17a, or zoccali_18b.

5.5. Metal-poor Stars in the Inner Galaxy

Contact Information: K. Schlaufman (Johns Hopkins University).

The oldest stars in the Milky Way are very metal-poor (i.e., $[Fe/H] < -2.0$) and may be found in the inner Galaxy (e.g., Tumlinson 2010). However, extreme reddening, extinction, and crowding in the inner Galactic bulge have made finding metal-poor stars in this region impossible with traditional techniques. Schlaufman & Casey (2014) published an efficient metal-poor star selection that uses only infrared photometry, thereby overcoming the previous barriers to the identification of metal-poor stars in the inner Galaxy. The targets in this program were selected following the pure-infrared metal-poor star selection from Schlaufman & Casey (2014) using the photometry from the Spitzer/IRAC Galactic Legacy Infrared Mid-Plane Survey Extraordinaire (GLIMPSE; Benjamin et al. 2003; Churchwell et al. 2009) and applying dereddening from high-resolution bulge-specific maps from Gonzalez et al. (2011, 2012) assuming the Nishiyama et al. (2009) extinction law. A restriction of $H \leq 12.5$ was applied. Observations from this project have PROGRAMNAME schlaufman_17a.

5.6. The Structure of the Ancient Milky Way

Contact Information: J. A. Kollmeier (Observatories of the Carnegie Institution for Science) and R. Poleski (Warsaw).

RR Lyrae (RRL) stars provide a unique view into the ancient interior of the Milky Way. In addition to being old stars, the pulsations of RRL stars have long allowed accurate distance estimates. The distance estimates can be combined with proper motions (Poleski et al. 2013, 2015) and radial velocities (from APOGEE) to obtain full six dimensional phase-space information for these stars. The goal of this project is to target a large sample of RRL stars identified by the Optical Gravitational Lensing Experiment (OGLE) survey in the Galactic bulge (Udalski et al. 1992) for radial velocity measurement with APOGEE-2S. In particular, this program was designed to penetrate the dust of the Milky Way to see the 3D structure of its old central component—to compare with theories of formation of the bulge. Targets were selected by applying the OGLE-

defined periods to the H -band period–luminosity relationship to predict the mean H -band magnitudes. All of the RRL stars from this program have bit 24 set in APOGEE2_TARGET1. Observations from this project have PROGRAMNAME kollmeier_17a.

The original main survey plan also included RRL observations (Z17), designed by the same Contributed Program PIs. Thus, for the purposes of analysis and selection, this Contributed Program and the main survey program are identical.

5.7. Low Metallicity Cepheids

Contact Information: R. Beaton (Princeton University and the Observatories of the Carnegie Institution for Science).

This Contributed Program has collected single-phase APOGEE-2S spectroscopy for the brightest and most well-studied Cepheids in the LMC. The APOGEE measurements can be combined with literature multiband optical to mid-infrared photometry to study trends in metallicity and the absolute magnitude dispersion of these stars against the mean Leavitt Law. The Cepheid sample was largely selected from the OGLE-III catalog of Cepheid variables in the LMC (Soszynski et al. 2008), but was supplemented with key calibrators used for the Cepheid-based extragalactic distance scale (Persson et al. 2004; Scowcroft et al. 2011, 2016). To obtain high S/N data, these stars are observed in two to three sequential visits and, thus, pipeline combined data are all at the same phase of the photometric light curve. As a result, the targets go to an H depth of a 3 visit field (using the mean magnitudes; Table 2). Additional fainter Cepheids were also targeted as part of this program, with the caveat that they may not reach an S/N of 100 per pixel. We caution that sometimes the observations were significantly distributed in time. The remaining fibers were back-filled with targets from the “TESS/APOGEE Survey” (Section 5.8) but only going to a depth of $H \sim 11$ mag. Observations from this project have PROGRAMNAME beaton_18a.

5.8. TESS/APOGEE Survey

Contact Information: J. Teske (Carnegie Institution For Science, Earth and Planets Laboratory), J. van Saders (University of Hawaii), and R. Beaton (Princeton University and the Observatories of the Carnegie Institution for Science).

This program intended to collect APOGEE-2S spectra of bright ($7 < H < 11$ mag) stars that fall within the 450 deg^2 of the Southern Ecliptic Pole, a region of the sky where NASA’s TESS satellite (Ricker et al. 2015) has had continuous 1 year coverage, and with the TESS extended mission will have an additional year of coverage. These APOGEE-2S data will be used to measure stellar parameters and chemical abundances. When combined with the precise TESS photometric light curves, these data will enable investigations of open questions about exoplanets, stellar astrophysics, and distance ladder calibration. Target selection was made via simple 2MASS color and magnitude cuts: $7 < H < 11$ and $J - K > 0.3$. As plates were drilled, target priorities were defined as: (1) subgiants where asteroseismic detections are expected, (2) asteroseismic dwarfs from the ATL (Schofield et al. 2019), (3) targets likely to be placed on 2 minutes cadence for planet searches based on the CTL (Stassun et al. 2018), (4) hot star seismic targets (exceptions to the color cut), and (5) bright giants. Fields from this program have the word “-O_TESS” appended at the end of

their field name. Observations from this project have PROGRAMNAME TeskeVanSaders_18a.

5.9. Carina Star-forming Complexes

Contact Information: A. Roman-Lopes (Universidad de La Serena).

The Carina star-forming complexes contain some of the most massive star-forming regions in the Milky Way. It is an ideal laboratory to test theories of the spatially segregated formation of stars and triggering mechanisms. This program takes advantage of the large FOV and multiplexing capability of the APOGEE-S spectrograph to confirm the massive nature of hot star candidates in the Galactic plane. The fields observed in this project are located in the vicinity and periphery of regions forming massive stars in the Carina star-forming complexes. The excellent spectral resolution provided by the APOGEE-2S instrument and the high S/N radial velocity measurements enabled us to obtain spectroscopic information of about 1750 candidate massive stars, a task virtually impossible using single-slit NIR spectroscopic facilities. Further details for this program are provided in Roman-Lopes et al. (2020). Observations from this project have PROGRAMNAME RomanLopes_18a.

5.10. Corona Australis Protocluster

Contact Information: A. Stutz (Universidad de Concepción).

This program aims at measuring the radial velocities of the young stellar population in the Corona Australis protocluster. The “Slingshot” mechanism proposes that young stars gain kinetic energy via gas filament oscillations (Stutz & Gould 2016; Boekholt et al. 2017; Stutz 2018). Ultimately, such oscillations may “eject” protostars from their dense gas cradles, cutting off the supply of gas to the new stars. The “Slingshot” scenario proposes that magnetically driven instabilities in the gas may be responsible for the oscillations. Whatever the ultimate oscillation mechanism, the APOGEE-2S Corona Australis RV measurements enable the dynamics of this protocluster to be compared to those of the Orion-A Integral Shaped Filament.

Targets for this program were selected from the Spitzer-based catalog of Corona Australis members assembled by Peterson et al. (2011). We prioritize all young stellar objects (Classes 0, I, II, and III) with $H < 14$, comprising a high-priority sample of 50 objects that are distributed across two plates to cover the full stellar population. Observations from this project have PROGRAMNAME stutz_18a.

5.11. CAPOS: The Bulge Cluster APOGEE Survey

Contact Information: D. Geisler (Universidad de Concepción and Universidad de La Serena).

The Galactic bulge hosts a large number of globular clusters (e.g., Harris 2010; Kharchenko et al. 2016). These clusters are powerful cosmological probes to investigate the formation and chemical evolution of this key Galactic component (APOGEE studies in individual stars include: Hasselquist et al. 2020; Rojas-Arriagada et al. 2020; Queiroz et al. 2020). Unfortunately, until recently, we have not been able to unleash the full power of the bulge globular clusters to help unravel its mysteries due to their high extinction, which strongly impedes optical observations (e.g., Gran et al. 2019; Palma et al. 2019). However, extinction effects are minimized by observing in the NIR, allowing us to fully exploit the bulge GC’s extraordinary archeological attributes. The bulge Cluster APOGEE Survey

(CAPOS) will observe 20 of the bona fide bulge globular clusters that were not included for the APOGEE-2 observations (see Z17; Masseron et al. 2019; Mészáros et al. 2020). Combining this Contributed Program with the APOGEE Main Survey bring the total number of bulge clusters targeted with APOGEE to 28, just over 50% of the known bulge clusters. CAPOS will supply almost 75% of the observed objects and build a legacy database of the bulge globular cluster system. This will provide much better and more self-consistent radial velocities and spectroscopic metallicities than currently available for all of the observed bulge globular clusters. These observations will permit investigation of many salient details of these systems like their chemistry, the existence and properties of multiple populations, and orbital properties, among others. Observations from this project have the PROGRAMNAME of geisler_18a, geisler_19a, geisler_19b, or geisler_20a.

5.12. Massive Stars in the SMC and LMC

Contact Information: M. Drout (University of Toronto).

Our goal was to conduct a wide and shallow survey of the evolved massive star populations (e.g., yellow supergiants, red supergiants, and luminous blue variables) of the Large and Small Magellanic Clouds (LMC and SMC) with APOGEE-S.

For targeting, we followed a procedure similar to that outlined in Neugent et al. (2010, 2012), who studied the red and yellow supergiants (RSGs and YSGs) of the LMC and SMC. We first selected all objects with a 2MASS H quality flag of “AAA” and a magnitude of $H_{2\text{MASS}} < 12.2$ that lie within 4 deg^2 of the LMC and SMC, respectively. Centers for each galaxy were defined as $(\alpha, \delta)_{\text{LMC}} = (05:23:34.5, -69:45:22)$ and $(\alpha, \delta)_{\text{SMC}} = (00:52:44.8, -72:49:43)$.

To separate likely LMC/SMC supergiants from foreground dwarfs in the FOV we use a combination of Gaia DR2 (Gaia Collaboration et al. 2018) proper motions/parallax values and radial velocities/spectroscopic classifications, when available. We assign probabilities of membership based on Gaia DR2 kinematics by the procedure described in O’Grady et al. (2020), which is based on that outlined in Helmi et al. (2018). In brief, we use a curated sample of highly probable LMC/SMC members to define a distribution in $(\mu_\alpha, \mu_\delta, \pi)$ followed by LMC/SMC members. Each 2MASS source described above is then cross-matched with Gaia DR2, and a χ^2 value is computed to assess the consistency of its proper motion and parallax with these distributions. For the purposes of targeting, we designate any star with a $\chi^2 < 6.25$ (indicating that the star falls within the region that contains 90% of LMC/SMC members) as having Gaia kinematics that are “consistent” with LMC/SMC membership. In addition, we cross-match all of the 2MASS sources with Simbad Wenger et al. (2000) in 2018 May in order to retrieve any existing radial velocity measurements for spectroscopic classifications. For the purposes of targeting we take any source with v_{rad} greater than 200 km s^{-1} and 135 km s^{-1} in the direction of the LMC and SMC, respectively, as having velocities consistent with membership in the Clouds (Neugent et al. 2010, 2012), while we discard any source with a ‘V’-type classification as a foreground star.

With these ancillary data in hand, all APOGEE fields were then assigned targets, moving through an ordered list of priorities until fiber capacity was reached. The ranked priorities for the LMC were as follows. In the following definitions, we take the dividing line between “blue/yellow” and red stars to be $J - K = 0.9 \text{ mag}$. This corresponds to an effective

temperature of ~ 4800 K and is taken as the rough dividing line between YSGs and RSGs in Neugent et al. (2012).

1. Stars that are listed as a confirmed YSG or RSG in the spectroscopic sample of Neugent et al. (2012) or as a confirmed or candidate Luminous Blue Variable.
2. Stars that are consistent with LMC membership based on both Gaia kinematics and an existing radial velocity, and have $H < 11.3$ mag.
3. Stars that are consistent with LMC membership based on both Gaia kinematics and an existing radial velocity, and have $H < 11.8$ mag.
4. Stars that are consistent with LMC membership based on Gaia kinematics, have no existing radial velocity data, and fall within the 2MASS color cuts defined by Neugent et al. (2012) in order to identify YSGs down to a completeness limit of $\sim 12M_{\odot}$, using the Geneva evolutionary models (Maeder & Meynet 2001) and ATLAS9 atmosphere models (Kurucz 1993).
5. Stars that are consistent with LMC membership based on Gaia kinematics, have no existing radial velocity data, and fall within the 2MASS color cuts defined by Neugent et al. (2012) to identify RSGs with minimal contamination from AGB stars.
6. Other blue/yellow stars with $H < 11.6$ that are consistent with LMC membership based on Gaia kinematics and have no existing radial velocity data.
7. Other red stars with $H < 10.8$ that are consistent with LMC membership based on Gaia kinematics and have no existing radial velocity data.
8. Any remaining stars with $H < 11.3$ that are consistent with LMC membership based on Gaia kinematics and have no existing radial velocity data.
9. Other blue/yellow stars with $H < 11.8$ or red stars with $H < 11.6$ that are consistent with LMC membership based on Gaia kinematics and have no existing radial velocity data.
10. Other blue/yellow stars with $H < 11.6$ or red stars with $H < 12.0$ that are consistent with LMC membership based on Gaia kinematics and have no existing radial velocity data.
11. Stars that are consistent with LMC membership based on Gaia kinematics and were classified as carbon stars in Simbad (Wenger et al. 2000). Note that objects with a listed spectral classification of “C” were explicitly excluded in all previous steps.

Priority listings for the SMC were entirely analogous. Main difference were that in Step 1 confirmed YSGs were added from Neugent et al. (2010), and in Steps 4 and 5 the H magnitudes were shifted by 0.4 mag in order to account for the difference in distance modulus between the LMC and SMC.

In total 16 LMC fields and 5 SMC fields were constructed and observed. Field centers were chosen to optimize the number of confirmed RSG, YSGs, and LBVs from the samples outlined in Steps 1 and 2, above, with over 97% being successfully placed. When filling fields we allowed the stars from these samples to be placed in multiple fields, when possible, while all other stars were placed only once. In practice, this optimized the number of targets observed while also providing multiple epochs for a subset of stars over the ~ 4 months in 2018–2019 when observations were carried out. Fields in dense regions of the clouds were typically filled

proceeding through only the first five steps above, while some sparser regions proceeded through all 11 steps.

Observations from this project have PROGRAMNAME Drout_18b.

5.13. Rosette Molecular Clouds

Contact Information: A. Stutz (Universidad de Concepción).

As with the Corona Australis program (see Section 5.10), this program seeks to measure radial velocities for young stellar objects (YSOs) to test the “Slingshot” model of star and cluster formation (Stutz & Gould 2016; Stutz 2018; Stutz et al. 2018). This program targets the protocluster associated with the Rosette molecular cloud. Targets were selected from the WISE-selected catalog of cluster members assembled by Cambrésy et al. (2013). Cross-matching with Gaia DR2 (Gaia Collaboration et al. 2018) and 2MASS (Skrutskie et al. 2006), targets were required to have parallaxes consistent with that of the complex (e.g., $d = 1.4\text{--}1.6$ kpc) and prioritized according to their H magnitude. Sources with $H < 12.2$ were assigned to a bright plate planned for a single 1 hr visit. Members with $13.3 > H > 12.2$, or suffering from a fiber collision with a brighter neighbor in the bright plate, were assigned to a “dim” plate planned for 3 hr of integration time. The faintest members ($14.7 > H > 13.3$) were assigned to spare fibers, but were expected to return spectra with very S/N. Observations from this project have PROGRAMNAME stutz_18b.

5.14. Carina Protocluster

Contact Information: A. Stutz (Universidad de Concepción).

These data will provide radial velocities (RVs) for the young star protocluster population in the Carina cloud complex ($d \sim 2.3$ kpc, $M_{\text{gas}} \sim 6.3 \times 10^5 M_{\odot}$). Carina’s morphology and high-mass star content both stand in sharp contrast to the well-studied Orion-A cluster. One of the major differences is that Carina samples the complete initial mass function. With ~ 90 massive stars, Carina has a cosmological relevance as a protocluster cloud at solar metallicity. With high radial velocity precision, detailed scrutiny of the dynamics of the protocluster via self-consistent and simultaneous modeling of the stellar and gas kinematics is enabled. APOGEE-2S provides the required radial velocity precision for this goal. By surveying the recently formed stars (ages ~ 2 Myr) and combining with Gaia, the observational basis required for theoretical dynamical modeling of this representative protocluster-forming region is established.

Targets were selected from the Spitzer-based catalog of Carina members assembled by Povich et al. (2011), after cross-matching to Gaia DR2 Gaia Collaboration et al. (2018) and 2MASS Skrutskie et al. (2006). Sources with $H < 12$ were prioritized for 2 hr of integration, while fainter sources were planned for as many as 6 hr of integration time. Observations from this project have PROGRAMNAME stutz_19a.

5.15. OB Stars

Contact Information: J. A. Kollmeier (The Observatories of the Carnegie Institution for Science), A. Tkachenko (KU Leuven), and C. Aerts (KU Leuven).

By obtaining high-resolution spectroscopy for intermediate- to high-mass stars (O and B spectral types), this program exploits the synergy between asteroseismology and stellar binarity to bring into focus key topics of stellar physics. The

ultimate goal is to obtain precise observational constraints on the angular momentum transport inside of these stars by combining asteroseismic inferences of the interior structure (where properties are determined through the interpretation of their gravity-mode oscillations) with high-precision radial velocity measurements and atmospheric properties for these stars. This sample was selected based on the type of variability imprinted on the high-precision TESS light curves of the proposed targets, and the sample itself is a healthy mix between single and binary star systems. The APOGEE-2S instrument plays a critical role in this project by offering: (1) preliminary orbital phase coverage for known binary stars, which will ultimately enable the disentangling of individual spectral contributions and the determination of atmospheric properties, and (2) another constraint on the binarity. If stars are determined to be single, then the spectra will allow for determination of their atmospheric parameters. Observations from this project have PROGRAMNAME kollmeier_19b.

5.16. LMC Substructures

Contact Information: Antonela Monachesi (Universidad de La Serena).

The Magellanic Clouds are important systems to study. Due to their proximity, we can investigate in great detail their formation, interaction, and evolution, which can be used together to place constraints on dwarf galaxy formation models. During the last decade, an increasing number of photometric surveys that cover both the main bodies of the Magellanic Clouds and their surroundings have uncovered many substructures extending out to several degrees from their centers (e.g., Mackey et al. 2016, 2018; Pieres et al. 2017; Nidever et al. 2019). Such discoveries have especially revealed the complexities of the LMC. More recently, Belokurov & Erkal (2019) used Gaia DR2 (Gaia Collaboration et al. 2018) to detect several substructures around the LMC out to a radius of 20° . These discoveries provide new insights that are fundamental to understand the formation and evolution of the Magellanic Clouds. The spectral resolution and FOV of the APOGEE-2S instrument are crucial to analyze these newly discovered features and understand their origin.

To select these targets we used Gaia DR2 (Gaia Collaboration et al. 2018) astrometry and 2MASS photometry (Skrutskie et al. 2006) available for these field targets. The data were filtered using the following restrictions: (1) $\pi < 0.2 \text{ mas yr}^{-1}$, (2) fractional parallax uncertainty of $\sigma_\pi/\pi < 3$, and (3) a color–magnitude box of $0.6 < J - K_s < 1.4 \text{ mag}$, and $12 < H < 15 \text{ mag}$. Since this sample did not fill the plates, different proper-motion cuts were used to select stars as back-fillers of lower priority. Observations from this project have PROGRAMNAME monachesi_19b.

5.17. Orion Nebula Cluster and Vela C

Contact Information: A. Stutz (Universidad de Concepción).

This program consists of two parts, a program in Orion and in Vela C. The latter program was developed in addition to the former to use all of the time allocated to the program. The Orion Nebula Cluster is forming within the Integral Shaped Filament and serves as a laboratory for star and cluster formation physics (Stutz et al. 2018). Based on APOGEE data, this team recently proposed the Slingshot model, in which the stars and cluster form on the oscillating Integral Shaped Filament (Stutz & Gould 2016; Stutz 2018). Even though

previous APOGEE data have been pivotal to the development of this model, a large fraction of the young stars (470 stars brighter than $H = 14 \text{ mag}$) do not yet have radial velocity measurements. Moreover, a substantial fraction of these are not detected in Gaia DR2 (Gaia Collaboration et al. 2018). The goal of this project is to obtain APOGEE-2S radial velocities to provide kinematic information for this young population.

We select young stellar objects (stars with disks) from the Spitzer-based catalog assembled by Megeath et al. (2012). We remove all young stellar objects that have been previously observed with APOGEE (Cottaar et al. 2014; Da Rio et al. 2017; Cottle et al. 2018; Kounkel et al. 2018, using both public and private data). We obtain a target list that is composed of sources with $H > 13 \text{ mag}$, as the previous surveys adopted this as their limit. Because this region is highly clustered, we use multiple overlapping plates to build the sample due to fiber collisions.

To utilize the remainder of the assigned nights, additional plates targeting the Vela C region were designed. These targets were selected using two sets of selection criteria: (1) membership as assessed from Gaia DR2 (Gaia Collaboration et al. 2018) parallaxes and proper motions; (2) near- and mid-infrared spectral energy distributions (SEDs), using photometry from 2MASS (Skrutskie et al. 2006) and Spitzer, indicative of being on the pre-main sequence. The SED-based selection was kindly provided by R. Gutermuth (private communication), following methods used to assemble the Spitzer Extended Solar Neighborhood Archive (Gutermuth et al. 2019). Observations from this project have PROGRAMNAME stutz_20a.

5.18. Carina Nebula Cluster

Contact Information: N. Medina (Universidad de Valparaíso).

The stars in formation and early stages of evolution, so called young stellar objects, undergo rapid structural changes, such as formation and destruction of the disks, jets, envelopes, flares, accretion, etc., and for these reasons the variation of their luminosity and colors is widely observed. Thus, the study of photometric variability is one of the most powerful sources of astrophysical information. Variability in the infrared fluxes, which detects young stellar objects at very early, obscured stages of evolution, has been found to be a very common characteristic among young stars. The “VISTA Variables in the Via Lactea survey” (VVV; Minniti et al. 2010) and its undergoing extension the “VISTA Variables in the Via Lactea Extended survey” (VVVX) are time-domain infrared surveys that provide the unique opportunity to investigate the connection between infrared variability and its underlying physics. Using the automated tool from Medina et al. (2018) we searched the Carina region for variable young stellar objects in K_s and created a catalog of candidate targets. APOGEE-2 spectroscopy complements photometric variability studies. The project will collect spectroscopy of ~ 1000 young stellar objects, covering the whole projected area of the Carina Nebula Complex. Spectroscopy allows validation of the photometric classification of the variable stars as young stellar objects, removing the AGB stars, novae, and long period variables, which show similar light-curve behavior, especially for high amplitude variables. Furthermore, the new class of “low amplitude eruptive variables” proposed by Medina et al. (2018) will be spectroscopically characterized for the first time. Emission features in the APOGEE spectra may reveal a high accretion rate and, thereby, improve the classification obtained

from the light curves. This can be used to constrain the possible triggered physical process, as well as will investigate the kinematic distribution of young stellar objects in the Carina region. The metallicity distribution of young stellar objects will allow for an outline of some possible differences in star formation processes within the complex. The observations from this project have PROGRAMNAME medina_20a.

5.19. NGC 6362 Cluster

Contact Information: José G. Fernández-Trincado (Universidad de Atacama).

NGC 6362 is a nearby low-mass, old stellar system with an intermediate metallicity; as such, it is a perfect tool to study the phenomenon of multiple stellar populations to large projected radius. Measurements from APOGEE-2S will place constraints on the extra-tidal population and, thus, will provide insight into its formation, evolution, chemistry, and kinematics, all of which are poorly understood at present. There was no compelling evidence for any significant extra-tidal population in NGC 6362 until recent work by Kundu et al. (2019). Kundu et al. (2019) claimed to have identified extra-tidal candidates using photometry and astrometry from Gaia DR2 (Gaia Collaboration et al. 2018) using color–magnitude and proper-motion constraints that maximized the contrast between cluster and field populations. This program aims to observe the bulk of the Gaia DR2 extra-tidal candidates as well as supplement the current APOGEE-2S sample of potential cluster members to trace the chemical and dynamical history of NGC 6362. Observations from this project have PROGRAMNAME fernandez_20a.

6. Summary

The second generation of the APOGEE project, APOGEE-2, includes an expansion of the survey to the Southern Hemisphere called APOGEE-2S, which observes the sky simultaneously with APOGEE-2N using a cloned spectrograph. This enabled APOGEE to truly map the Milky Way in a panoramic manner, while putting special attention to the dust-hidden inner regions of the Milky Way, which is crucial to make a comprehensive chemodynamical analysis of the Milky Way.

Z17 presented the targeting selection strategy used for APOGEE-2 (both North and South counterparts), which has been modified and updated as the survey has progressed. Throughout this paper we present the final targeting strategy of APOGEE-2S, with special attention to the changes applied since Z17. First, we briefly described the main concepts involved in the process of target selection for all components of APOGEE. Then, we presented the main motivations for changing our target selection with respect to the one presented in Z17, which involved internal evaluations to maximize our ability to reach our science goals, the use of data from new external surveys in our selection methods, and the alterations of our observing schedule. Probably the latter is the most important motivation for this paper, since our original plan was designed for 1493 visits obtained throughout 320 observing nights. However, as explained in Section 4.1, our observing efficiency and the observing schedule changed significantly over the course of the survey. The global spread of the COVID-19 pandemic in early 2020 resulted in the loss of 77 observing nights, which was compensated for by the extension that was granted to APOGEE-2S that included 88 nights granted for the end of year 2020. With all of these

changes our final observing strategy encompassed 2120 total planned visits, obtained throughout 352 observing nights, which represent 42% more than the original observing plan.

The other subsections of Section 4 summarize the main changes applied to the constituent programs of the main survey. The bulge program was unintentionally filled with stars fainter than needed given our planned visits per field, but thanks to a modification in the plan and increment in our observing efficiency, we obtained a bulge coverage that was significantly deeper than our original bulge program. For the halo, thanks to the extra nights granted, we could add new fields meant to target both halo and stellar stream targets, and using the results obtained from APOGEE2-N we could improve our halo selection method and increase our efficiency to target distant stars. The other project that was significantly modified was the Magellanic Cloud program for which we practically doubled the number of fields in our observing plan thanks to the nights allocated for the end of year 2020. Other changes to our observing plan involve the inclusion of the Fornax dSph galaxy, and new globular and open clusters that allowed us to fine-tune our metallicity calibration. We also present our definitive observing field plan map, and provide the final version of the list of targeting flags used in this survey so that the user can identify the purpose for which all of the different targets of APOGEE-2S were intended.

Finally, we present for the first time the list of contributed programs to APOGEE-2S, which are allocated either through the Chilean Time Allocation Committee (CNTAC) or by the Observatories of the Carnegie Institution of Science (CIS) TAC. These 19 programs are designed by the PI responsible and the APOGEE-2S team only perform checks of observability and plugability. Each program is scheduled for specific nights, and the total nights assigned to contributed programs in APOGEE-2S was 104, which represents $\sim 23\%$ of the total observing time of the survey. The contributed program section provides small descriptions of each project along with the contact information from the PI, whereas the overall coverage of contributed programs is shown in Figure 5.

The APOGEE project thanks Jeff Munn (NOFS) for collecting Washington + DDO51 imaging for large areas of the sky. The authors also recognize contributions from prior members of the targeting team and the members of the science working groups in both APOGEE-1 and APOGEE-2. We graciously thank the staff at Las Campanas Observatory and the APOGEE-2S Observing team for both their dedication and their remarkable ability to exceed themselves without needing to. We also warmly recognize the APOGEE-S Operations team for their diligence, the Carnegie Observatories Telescope Allocation staff, the members of the CNTAC, and the SDSS Plate Shop for their enduring patience. We thank the SDSS-IV Data Team for thinking about and then handling so many details and doing so without a complaint, albeit often with a stroopwafel. We thank the SDSS-IV Management Committee and all SDSS-IV leadership whose commitment to SDSS-IV is literally the glue that keeps the project going. Lastly, we warmly thank Jim Gunn and Jill Knapp for the remarkable manner in which they have and continue to impact the world around them.

This work has been partially funded by the BASAL Center for Astrophysics and Associated Technologies AFB-170002. Support for this work was provided by NASA through Hubble Fellowship grant #51386.01 awarded to R.L.B. by the Space

Telescope Science Institute, which is operated by the Association of Universities for Research in Astronomy, Inc., for NASA, under contract NAS 5-26555. K.R.C. acknowledges support provided by the NSF through grant AST-1449476. S.R. M. acknowledges support through NSF grants AST-1616636 and AST-1909497. The research leading to these results has (partially) received funding from the European Research Council (ERC) under the European Union’s Horizon 2020 research and innovation program (grant agreement N°670519: MAMSIE), from the KU Leuven Research Council (grant C16/18/005: PARADISE), as well as from the BELgian federal Science Policy Office (BELSPO) through PRODEX grant PLATO (C.A. and A.T.). J.B. and N.M. are supported by the ANID – Millennium Science Initiative Program – ICN12_009 awarded to the Millennium Institute of Astrophysics MAS. N.M. also acknowledges support through a Fellowship for National PhD students from ANID, grant number 21181952. J.D. and P.M.F. acknowledge support for this research from the National Science Foundation AAG and REU programs (AST-1311835, AST-1715662, PHY-1358770, and PHY-1659444). J.G.F.-T. is supported by FONDECYT No. 3180210 and Becas Iberoamérica Investigador 2019, Banco Santander Chile. D.G. acknowledges financial support from the Dirección de Investigación y Desarrollo de la Universidad de La Serena through the Programa de Incentivo a la Investigación de Académicos (PIA-DIDULS). S.H. is supported by an NSF Astronomy and Astrophysics Postdoctoral Fellowship under award AST-1801940. D.M. acknowledges support by Proyecto FONDECYT No. 1170121. R.R.M. acknowledges support from FONDECYT project N°1170364. A.R.A. acknowledges support from FONDECYT through grant 3180203. A.R.-L. acknowledges financial support provided in Chile by the National Agency for Research and Development (ANID) through the FONDECYT project 1170476 and by the QUIMAL project 130001. A.M.S. gratefully acknowledges funding support through Fondecyt Regular (project code1180350). G.Z. acknowledges support from the NSF through grants AST-1203017 and AST-1911129. A.M. acknowledges support from FONDECYT Regular grant 1212046 and funding from the Max Planck Society through a “PartnerGroup grant.” M.Z. acknowledges support from FONDECYT Regular grant 1191505.

Funding for the Sloan Digital Sky Survey IV has been provided by the Alfred P. Sloan Foundation, the U.S. Department of Energy Office of Science, and the Participating Institutions. SDSS-IV acknowledges support and resources from the Center for High-Performance Computing at the University of Utah. The SDSS website is www.sdss.org.

SDSS-IV is managed by the Astrophysical Research Consortium for the Participating Institutions of the SDSS Collaboration including the Brazilian Participation Group, the Carnegie Institution for Science, Carnegie Mellon University, the Chilean Participation Group, the French Participation Group, Harvard-Smithsonian Center for Astrophysics, Instituto de Astrofísica de Canarias, The Johns Hopkins University, Kavli Institute for the Physics and Mathematics of the Universe (IPMU)/University of Tokyo, Lawrence Berkeley National Laboratory, Leibniz Institut für Astrophysik Potsdam (AIP), Max-Planck-Institut für Astronomie (MPIA Heidelberg), Max-Planck-Institut für Astrophysik (MPA Garching), Max-Planck-Institut für Extraterrestrische Physik (MPE), National Astronomical Observatories of China, New Mexico State University,

New York University, University of Notre Dame, Observatório Nacional/MCTI, The Ohio State University, Pennsylvania State University, Shanghai Astronomical Observatory, United Kingdom Participation Group, Universidad Nacional Autónoma de México, University of Arizona, University of Colorado Boulder, University of Oxford, University of Portsmouth, University of Utah, University of Virginia, University of Washington, University of Wisconsin, Vanderbilt University, and Yale University.

This publication makes use of data products from the Two Micron All Sky Survey, which is a joint project of the University of Massachusetts and the Infrared Processing and Analysis Center/California Institute of Technology, funded by the National Aeronautics and Space Administration and the National Science Foundation.

This work is based, in part, on observations made with the Spitzer Space Telescope, which is operated by the Jet Propulsion Laboratory, California Institute of Technology under a contract with NASA.

This publication makes use of data products from the Wide-field Infrared Survey Explorer (Wright et al. 2010), which is a joint project of the University of California, Los Angeles, and the Jet Propulsion Laboratory/California Institute of Technology, funded by the National Aeronautics and Space Administration, and NEOWISE, which is a project of the Jet Propulsion Laboratory/California Institute of Technology. WISE and NEOWISE are funded by the National Aeronautics and Space Administration

This work has made use of data from the European Space Agency (ESA) mission Gaia (<https://www.cosmos.esa.int/gaia>), processed by the Gaia Data Processing and Analysis Consortium (DPAC, <https://www.cosmos.esa.int/web/gaia/dpac/consortium>). Funding for the DPAC has been provided by national institutions, in particular the institutions participating in the Gaia Multilateral Agreement.

This research has made use of NASAs Astrophysics Data System.

Many of the acknowledgments were compiled using the Astronomy Acknowledgement Generator.

This research has made use of the SIMBAD database, operated at CDS, Strasbourg, France. The original description of the SIMBAD service was published in Wenger et al. (2000).

This research has made use of the VizieR catalog access tool, CDS, Strasbourg, France (DOI:10.26093/cds/vizieR). The original description of the VizieR service was published Ochsenein et al. (2000).

Facilities: Du Pont (APOGEE), Sloan (APOGEE), Spitzer, WISE, 2MASS, SkyMapper, Gaia.

Software: Astropy (Astropy Collaboration et al. 2013, 2018), NumPy (van der Walt et al. 2011; Harris et al. 2020), TopCat (Taylor 2005).







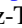
Appendix GLOSSARY

This Glossary contains SDSS- and APOGEE-specific terminology appearing in this paper and throughout the data documentation.

1-Meter Target: Target observed with the NMSU 1 m telescope (TELESCOPE tag of “apo1m”), which has a single fiber connection to the APOGEE-2N instrument. The NMSU 1 m telescope is described in Holtzman et al. (2010) with the

- reduction specific to its connection to the APOGEE-N instrument given in Holtzman et al. (2015).
- Ancillary Target*: Target observed as part of an approved Ancillary Science Program. Ancillary Science Programs from APOGEE-1 are described in Z13 and from APOGEE-2 in R. Beaton et al. (submitted; AAS29028).
- APO*: Apache Point Observatory; site of the Sloan Foundation 2.5 m telescope (Gunn et al. 2006) on which the APOGEE-N spectrograph operates.
- ASPCAP*: The APOGEE Stellar Parameters and Chemical Abundances Pipeline; the analysis software that calculates basic stellar parameters (T_{eff} , $\log g$, $[\text{Fe}/\text{H}]$, $[\alpha/\text{Fe}]$, $[\text{C}/\text{Fe}]$, $[\text{N}/\text{Fe}]$) and elemental abundances (Holtzman et al. 2015; García Pérez et al. 2016).
- BTX*: The Bright Time Extension, an APOGEE-2N program executed in the last 1.5 years of the APOGEE-2 Survey.
- CIS*: The Carnegie Institution for Science or CIS is an SDSS-IV partner and operates the Las Campanas Observatory in Chile.
- Cohort*: Set of targets in the same field that are observed together on all of their visits. A given plate may have multiple cohorts on it.
- Contributed Program*: Term for programs allocated to Principal Investigators by the CIS or CNTAC but whose data are contributed to the APOGEE-2 survey. These data appear in SDSS data releases, but their targeting was performed by the PIs. These programs are described in this work.
- CNTAC*: The Chilean National Telescope Allocation Committee, which allocates observing resources to the Chilean community.
- Design*: Set of targets drilled together on a plate, consisting of up to one each of short, medium, and long cohorts. A design is identified by an integer Design ID. Changing a single target on a design results in a new design.
- Design ID*: Unique integer assigned to each design.
- Drill Angle*: Hour angle (distance from the meridian) at which a plate is drilled to be observed. This places the fiber holes in a way that accounts for differential refraction across the FOV.
- External Program*: General term for programs and targets observed during the APOGEE-2S time allocated by the Carnegie Observatories (OCIS) or the Chilean Time Allocation Committee (CNTAC). These targets will not be included in the SDSS data set.
- Fiber Collision*: A situation in which two targets, separated by less than the protective ferrule around the fibers, are included in the same design. The higher priority target is drilled on the plate(s); the lower priority target is removed.
- Fiber ID*: Integer (1–300) corresponding to the rank-ordered spectrum on the detector. Fiber IDs can vary from visit to visit for a given star.
- Field*: Location on the sky, defined by central coordinates and a plate radius.
- GAP*: The K2 Galactic Astrophysics Program, which is described in Stello et al. (2017).
- LCO*: Las Campanas Observatory, site of the Irénée du Pont 2.5 m telescope (Bowen & Vaughan 1973) on which the APOGEE-S spectrograph operates.
- Location ID*: Unique integer assigned to each field on the sky.
- Main Red Star Sample*: The sample drawn from a simple selection function defined by magnitude and color that comprises the bulk of the APOGEE program. This program is explained in Z13 and Z17.
- MaNGA*: Mapping Nearby Galaxies at Apache Point Observatory; An SDSS-IV program described in Bundy et al. (2015).
- MaStar*: The MaNGA Stellar Program; a program within the MaNGA Survey with the objective of constructing a high-fidelity stellar library. An overview of the project and its first data release is described in Yan et al. (2019).
- POI*: Photometric Object of Interest; an umbrella term for stars targeted due to their Kepler, K2, or TESS light curves.
- Plate*: Piece of aluminum with a design drilled into it. Note that while “plate” is often used interchangeably with “design,” multiple plates may exist for the same design—e.g., plates with a common design but drilled for different hour angles.
- Plate ID*: Unique integer assigned to each plate.
- RJCE*: The Rayleigh–Jeans Color Excess method, a technique used to estimate the line-of-sight reddening to a star (Majewski et al. 2011). APOGEE-2 uses this method to estimate intrinsic colors for many potential targets (for details see Z13, Z17).
- Sky Targets*: Empty regions of sky on which a fiber is placed to collect a spectrum used to remove the atmospheric airglow lines and sky background from the target spectra observed simultaneously with the same plate.
- Special Targets*: General term for targets selected with criteria other than the color and magnitude criteria of the main red giant sample. For example, special targets include ancillary science program targets and calibration cluster members.
- Targeting Flag and Bits*: A targeting “flag” refers to one of the three long integers assigned to every target in a design, each made up of 31 “bits” that correspond to particular selection or assignment criteria. APOGEE-2’s flags are named APOGEE2_TARGET1, APOGEE2_TARGET2, APOGEE2_TARGET3, and APOGEE2_TARGET4; see Table 1 for a list of the bits as of this publication.
- Telluric Standards*: Hot blue stars observed on a plate to derive corrections for the telluric absorption lines.
- Visit*: The base unit of observation, equivalent to approximately one hour of on-sky integration (but this can vary; see Section 2.1) and comprising a single epoch. Repeated visits are used to both build up signal and provide a measure of spectral and RV stability.
- Washington+DDO51*: Also “W + D photometry”; adopted abbreviation for the combination of Washington M and T_2 photometry (Canterna 1976) with DDO51 photometry (McClure 1973), used in the photometric classification of dwarf/giant stars (Majewski et al. 2000).

ORCID iDs

- Felipe A. Santana  <https://orcid.org/0000-0002-4023-7649>
 Rachael L. Beaton  <https://orcid.org/0000-0002-1691-8217>
 Kevin R. Covey  <https://orcid.org/0000-0001-6914-7797>
 Julia E. O’Connell  <https://orcid.org/0000-0003-2321-950X>
 Penélope Longa-Peña  <https://orcid.org/0000-0001-9330-5003>
 Roger Cohen  <https://orcid.org/0000-0002-2970-7435>
 José G. Fernández-Trincado  <https://orcid.org/0000-0003-3526-5052>

Christian R. Hayes  <https://orcid.org/0000-0003-2969-2445>
 Gail Zasowski  <https://orcid.org/0000-0001-6761-9359>
 Jennifer S. Sobeck  <https://orcid.org/0000-0002-4989-0353>
 Steven R. Majewski  <https://orcid.org/0000-0003-2025-3147>
 S. D. Chojnowski  <https://orcid.org/0000-0001-9984-0891>
 Nathan De Lee  <https://orcid.org/0000-0002-3657-0705>
 Ryan J. Oelkers  <https://orcid.org/0000-0002-0582-1751>
 Guy S. Stringfellow  <https://orcid.org/0000-0003-1479-3059>
 Borja Anguiano  <https://orcid.org/0000-0001-5261-4336>
 Peter M. Frinchaboy  <https://orcid.org/0000-0002-0740-8346>
 Sten Hasselquist  <https://orcid.org/0000-0001-5388-0994>
 Jennifer A. Johnson  <https://orcid.org/0000-0001-7258-1834>
 Juna A. Kollmeier  <https://orcid.org/0000-0001-9852-1610>
 David L. Nidever  <https://orcid.org/0000-0002-1793-3689>
 Adrian M. Price-Whelan  <https://orcid.org/0000-0003-0872-7098>
 Alvaro Rojas-Arriagada  <https://orcid.org/0000-0003-0208-8854>
 Mathias Schultheis  <https://orcid.org/0000-0002-6590-1657>
 Matthew Shetrone  <https://orcid.org/0000-0003-0509-2656>
 Joshua D. Simon  <https://orcid.org/0000-0002-4733-4994>
 Conny Aerts  <https://orcid.org/0000-0003-1822-7126>
 Jura Borissova  <https://orcid.org/0000-0002-5936-7718>
 Doug Geisler  <https://orcid.org/0000-0002-3900-8208>
 C. Y. Law  <https://orcid.org/0000-0003-1964-970X>
 Nicolas Medina  <https://orcid.org/0000-0002-4684-1927>
 Dante Minniti  <https://orcid.org/0000-0002-7064-099X>
 Antonela Monachesi  <https://orcid.org/0000-0003-2325-9616>
 Ricardo R. Muñoz  <https://orcid.org/0000-0002-0810-5558>
 Radosław Poleski  <https://orcid.org/0000-0002-9245-6368>
 Alexandre Roman-Lopes  <https://orcid.org/0000-0002-1379-4204>
 Kevin C. Schlafman  <https://orcid.org/0000-0001-5761-6779>
 Amelia M. Stutz  <https://orcid.org/0000-0003-2300-8200>
 Jennifer L. Van Saders  <https://orcid.org/0000-0002-4284-8638>
 Alycia J. Weinberger  <https://orcid.org/0000-0001-6654-7859>
 Manuela Zoccali  <https://orcid.org/0000-0002-5829-2267>

References

Abolfathi, B., Aguado, D. S., Aguilar, G., et al. 2018, *ApJS*, 235, 42
 Ahumada, R., Allende Prieto, C., Almeida, A., et al. 2020, *ApJS*, 249, 3
 Altman, M., Roeser, S., Demleitner, M., Bastian, U., & Schilbach, E. 2017, *A&A*, 600, L4
 Anguiano, B., Zucker, D. B., Scholz, R. D., et al. 2015, *MNRAS*, 451, 1229
 Astropy Collaboration, Price-Whelan, A. M., Sipőcz, B. M., et al. 2018, *AJ*, 156, 123
 Astropy Collaboration, Robitaille, T. P., Tollerud, E., et al. 2013, *A&A*, 558, A33
 Baumgardt, H., Hilker, M., Sollima, A., & Bellini, A. 2019, *MNRAS*, 482, 5138
 Belokurov, V., Zucker, D. B., Evans, N. W., et al. 2006, *ApJL*, 642, L137
 Beaton, R. L., Oelkers, R. J., Hayes, C. R., et al. 2021, arXiv:2108.11907
 Belokurov, V. A., & Erkal, D. 2019, *MNRAS*, 482, L9
 Benjamin, R. A., Churchwell, E., Babler, B. L., et al. 2003, *PASP*, 115, 953
 Benjamin, R. A., Churchwell, E., Babler, B. L., et al. 2005, *ApJL*, 630, L149
 Blanton, M. R., Bershady, M. A., Abolfathi, B., et al. 2017, *AJ*, 154, 28
 Boekholt, T. C. N., Stutz, A. M., Fellhauer, M., Schleicher, D. R. G., & Matus Carrillo, D. R. 2017, *MNRAS*, 471, 3590

Bonaca, A., Conroy, C., Price-Whelan, A. M., & Hogg, D. W. 2019, *ApJL*, 881, L37
 Bonanos, A. Z., Massa, D. L., Sewilo, M., et al. 2009, *AJ*, 138, 1003
 Borissova, J., Roman-Lopes, A., Covey, K., et al. 2019, *AJ*, 158, 46
 Bowen, I. S., & Vaughan, A. H. 1973, *ApOpt*, 12, 1430
 Bundy, K., Bershady, M. A., Law, D. R., et al. 2015, *ApJ*, 798, 7
 Cañas, C. I., Stefansson, G., Monson, A. J., et al. 2019a, *ApJL*, 877, L29
 Cañas, C. I., Wang, S., Mahadevan, S., et al. 2019b, *ApJL*, 870, L17
 Cambrésy, L., Marton, G., Feher, O., Tóth, L. V., & Schneider, N. 2013, *A&A*, 557, A29
 Canterna, R. 1976, *AJ*, 81, 228
 Carpenter, J., Hillenbrand, L., Mamajek, E., & Meyer, M. 2005, Spitzer Proposal, 20069
 Carpenter, J., Hillenbrand, L., Mamajek, E., Meyer, M., & Slesnick, C. 2006a, Spitzer Proposal, 30091
 Carpenter, J. M., Mamajek, E. E., Hillenbrand, L. A., & Meyer, M. R. 2006b, *ApJL*, 651, L49
 Carpenter, J. M., Mamajek, E. E., Hillenbrand, L. A., & Meyer, M. R. 2009, *ApJ*, 705, 1646
 Casagrande, L., Wolf, C., Mackey, A. D., et al. 2019, *MNRAS*, 482, 2770
 Choi, J., Dotter, A., Conroy, C., et al. 2016, *ApJ*, 823, 102
 Chojnowski, S. D., Hubrig, S., & Hasselquist, S. 2019, *ApJL*, 873, L5
 Chojnowski, S. D., Hubrig, S., Hasselquist, S., et al. 2020, *MNRAS*, 496, 832
 Churchwell, E., Babler, B. L., Meade, M. R., et al. 2009, *PASP*, 121, 213
 Clark Cunningham, J. M., Rawls, M. L., Windemuth, D., et al. 2019, *AJ*, 158, 106
 Contreras Ramos, R., Zoccali, M., Rojas, F., et al. 2017, *A&A*, 608, A140
 Cottaar, M., Covey, K. R., Meyer, M. R., et al. 2014, *ApJ*, 794, 125
 Cottle, J. N., Covey, K. R., Suárez, G., et al. 2018, *ApJS*, 236, 27
 Da Rio, N., Tan, J. C., Covey, K. R., et al. 2017, *ApJ*, 845, 105
 Donaldson, J. K., Weinberger, A. J., Gagné, J., Boss, A. P., & Keiser, S. A. 2017, *ApJ*, 850, 11
 Donor, J., Frinchaboy, P. M., Cunha, K., et al. 2018, *AJ*, 156, 142
 Donor, J., Frinchaboy, P. M., Cunha, K., et al. 2020, *AJ*, 159, 199
 Dotter, A. 2016, *ApJS*, 222, 8
 Eilers, A.-C., Hogg, D. W., Rix, H.-W., & Ness, M. K. 2019, *ApJ*, 871, 120
 Eisenstein, D. J., Weinberg, D. H., Agol, E., et al. 2011, *AJ*, 142, 72
 Fernández-Alvar, E., Fernández-Trincado, J. G., Moreno, E., et al. 2019, *MNRAS*, 487, 1462
 Fernández-Trincado, J. G., Robin, A. C., Vieira, K., et al. 2015, *A&A*, 583, A76
 Frankel, N., Sanders, J., Rix, H.-W., Ting, Y.-S., & Ness, M. 2019, *ApJ*, 884, 99
 Frinchaboy, P. M., Thompson, B., Jackson, K. M., et al. 2013, *ApJL*, 777, L1
 Gaia Collaboration, Brown, A. G. A., Vallenari, A., et al. 2016b, *A&A*, 595, A2
 Gaia Collaboration, Brown, A. G. A., Vallenari, A., et al. 2018, *A&A*, 616, A1
 Gaia Collaboration, Prusti, T., de Bruijne, J. H. J., et al. 2016a, *A&A*, 595, A1
 García Pérez, A. E., Allende Prieto, C., Holtzman, J. A., et al. 2016, *AJ*, 151, 144
 Geisler, D. 1984, *PASP*, 96, 723
 Gonzalez, O. A., Minniti, D., Valenti, E., et al. 2018, *MNRAS*, 481, L130
 Gonzalez, O. A., Rejkuba, M., Zoccali, M., Valenti, E., & Minniti, D. 2011, *A&A*, 534, A3
 Gonzalez, O. A., Rejkuba, M., Zoccali, M., et al. 2012, *A&A*, 543, A13
 Gran, F., Zoccali, M., Contreras Ramos, R., et al. 2019, *A&A*, 628, A45
 Griffith, E., Weinberg, D. H., Johnson, J. A., et al. 2021, *ApJ*, 909, 77
 Gullieuszik, M., Held, E. V., Rizzi, L., et al. 2007, *A&A*, 467, 1025
 Gunn, J. E., Siegmund, W. A., Mannery, E. J., et al. 2006, *AJ*, 131, 2332
 Gutermuth, R., Dunham, M., & Offner, S. 2019, AAS Meeting, 233, 367.10
 Harris, C. R., Millman, K. J., van der Walt, S. J., et al. 2020, *Natur*, 585, 357
 Harris, W. E. 2010, arXiv:1012.3224
 Hasselquist, S., Carlin, J. L., Holtzman, J. A., et al. 2019b, *ApJ*, 872, 58
 Hasselquist, S., Holtzman, J. A., Shetrone, M., et al. 2019a, *ApJ*, 871, 181
 Hasselquist, S., Zasowski, G., Feuillet, D. K., et al. 2020, *ApJ*, 901, 109
 Hayes, C. R., Law, D. R., & Majewski, S. R. 2018a, *ApJL*, 867, L20
 Hayes, C. R., Majewski, S. R., Hasselquist, S., et al. 2018b, *ApJL*, 859, L8
 Hayes, C. R., Majewski, S. R., Hasselquist, S., et al. 2020, *ApJ*, 889, 63
 Helmi, A., Babusiaux, C., Koppelman, H. H., et al. 2018, *Natur*, 563, 85
 Hodge, P. W. 1961, *AJ*, 66, 83
 Holtzman, J. A., Harrison, T. E., & Coughlin, J. L. 2010, *AdAst*, 2010, 46
 Holtzman, J. A., Hasselquist, S., Shetrone, M., et al. 2018, *AJ*, 156, 125
 Holtzman, J. A., Shetrone, M., Johnson, J. A., et al. 2015, *AJ*, 150, 148
 Hon, M., Stello, D., García, R. A., et al. 2019, *MNRAS*, 485, 5616
 Horta, D., Schiavon, R. P., Mackereth, J. T., et al. 2020, *MNRAS*, 493, 3363
 Howell, S. B., Sobeck, C., Haas, M., et al. 2014, *PASP*, 126, 398

- Ibata, R. A., Bellazzini, M., Malhan, K., Martin, N., & Bianchini, P. 2019, *NatAs*, **3**, 667
- Johnson, C. I., Dupree, A. K., Mateo, M., et al. 2020, *AJ*, **159**, 254
- Jönsson, H., Holtzman, J. A., Prieto, C. A., et al. 2020, *AJ*, **160**, 120
- Kamath, D., Wood, P. R., & Van Winckel, H. 2014, *MNRAS*, **439**, 2211
- Kamath, D., Wood, P. R., & Van Winckel, H. 2015, *MNRAS*, **454**, 1468
- Keller, S. C., Schmidt, B. P., Bessell, M. S., et al. 2007, *PASA*, **24**, 1
- Kharchenko, N. V., Piskunov, A. E., Schilbach, E., Röser, S., & Scholz, R. D. 2016, *A&A*, **585**, A101
- Koposov, S. E., Belokurov, V., Li, T. S., et al. 2019, *MNRAS*, **485**, 4726
- Kounkel, M., Covey, K., Suárez, G., et al. 2018, *AJ*, **156**, 84
- Kunder, A., Kordopatis, G., Steinmetz, M., et al. 2017, *AJ*, **153**, 75
- Kundu, R., Fernández-Trincado, J. G., Minniti, D., et al. 2019, *MNRAS*, **489**, 4565
- Kurucz, R. L. 1993, in IAU Colloq. 138, Peculiar versus Normal Phenomena in A-type and Related Stars, ed. M. M. Dworetzky, F. Castelli, & R. Faraggiana (San Francisco, CA: ASP), 87
- Launhardt, R., Zylka, R., & Mezger, P. G. 2002, *A&A*, **384**, 112
- Lemasle, B., de Boer, T. J. L., Hill, V., et al. 2014, *A&A*, **572**, A88
- Letarte, B., Hill, V., Tolstoy, E., et al. 2010, *A&A*, **523**, A17
- Lewis, H. M., Anguiano, B., Stassun, K. G., et al. 2020, *ApJL*, **900**, L43
- Mackereth, J. T., & Bovy, J. 2020, *MNRAS*, **492**, 3631
- Mackereth, J. T., Bovy, J., Leung, H. W., et al. 2019a, *MNRAS*, **489**, 176
- Mackereth, J. T., Miglio, A., Elsworth, Y., et al. 2021, *MNRAS*, **502**, 1947
- Mackereth, J. T., Schiavon, R. P., Pfeffer, J., et al. 2019b, *MNRAS*, **482**, 3426
- Mackey, A. D., Koposov, S. E., Erkal, D., et al. 2016, *MNRAS*, **459**, 239
- Mackey, D., Koposov, S., Da Costa, G., et al. 2018, *ApJL*, **858**, L21
- Maeder, A., & Meynet, G. 2001, *A&A*, **373**, 555
- Majewski, S. R., Osthheimer, J. C., Kunkel, W. E., & Patterson, R. J. 2000, *AJ*, **120**, 2550
- Majewski, S. R., Schiavon, R. P., Frinchaboy, P. M., et al. 2017, *AJ*, **154**, 94
- Majewski, S. R., Skrutskie, M. F., Weinberg, M. D., & Osthheimer, J. C. 2003, *ApJ*, **599**, 1082
- Majewski, S. R., Zasowski, G., & Nidever, D. L. 2011, *ApJ*, **739**, 25
- Marconi, M., Musella, I., Di Criscienzo, M., et al. 2014, *MNRAS*, **444**, 3809
- Masseron, T., García-Hernández, D. A., Mészáros, S., et al. 2019, *A&A*, **622**, A191
- Mazzola, C. N., Badenes, C., Moe, M., et al. 2020, *MNRAS*, **499**, 1607
- McClure, R. D. 1973, in IAU Symp. 50, Spectral Classification and Multicolour Photometry, ed. C. Fehrenbach & B. E. Westerlund (Dordrecht: Reidel), 162
- Medina, N., Borissova, J., Bayo, A., et al. 2018, *ApJ*, **864**, 11
- Megeath, S. T., Gutermuth, R., Muzerolle, J., et al. 2012, *AJ*, **144**, 192
- Mészáros, S., Masseron, T., García-Hernández, D. A., et al. 2020, *MNRAS*, **492**, 1641
- Minniti, D., Lucas, P. W., Emerson, J. P., et al. 2010, *NewA*, **15**, 433
- Morris, M., & Serabyn, E. 1996, *ARA&A*, **34**, 645
- Muñoz, R. R., Côté, P., Santana, F. A., et al. 2018, *ApJ*, **860**, 65
- Muñoz, R. R., Frinchaboy, P. M., Majewski, S. R., et al. 2005, *ApJL*, **631**, L137
- Neugent, K. F., Massey, P., Skiff, B., et al. 2010, *ApJ*, **719**, 1784
- Neugent, K. F., Massey, P., Skiff, B., & Meynet, G. 2012, *ApJ*, **749**, 177
- Nidever, D. L., Hasselquist, S., Hayes, C. R., et al. 2020, *ApJ*, **895**, 88
- Nidever, D. L., Holtzman, J. A., Allende Prieto, C., et al. 2015, *AJ*, **150**, 173
- Nidever, D. L., Olsen, K., Choi, Y., et al. 2019, *ApJ*, **874**, 118
- Nikolaev, S., & Weinberg, M. D. 2000, *ApJ*, **542**, 804
- Nishiyama, S., Tamura, M., Hatano, H., et al. 2009, *ApJ*, **696**, 1407
- Nogueras-Lara, F., Schödel, R., Gallego-Calvente, A. T., et al. 2019, *NatAs*, **4**, 377
- Ochsenbein, F., Bauer, P., & Marcout, J. 2000, *A&AS*, **143**, 23
- O'Grady, A. J. G., Drout, M. R., Shappee, B. J., et al. 2020, *ApJ*, **901**, 135
- Olsen, K. A. G., Zaritsky, D., Blum, R. D., Boyer, M. L., & Gordon, K. D. 2011, *ApJ*, **737**, 29
- Owen, R. E., Siegmund, W. A., Limmongkol, S., & Hull, C. L. 1994, *Proc. SPIE*, **2198**, 110
- Palma, T., Minniti, D., Alonso-García, J., et al. 2019, *MNRAS*, **487**, 3140
- Persson, S. E., Madore, B. F., Krzemiński, W., et al. 2004, *AJ*, **128**, 2239
- Peterson, D. E., Caratti o Garatti, A., Bourke, T. L., et al. 2011, *ApJS*, **194**, 43
- Pieres, A., Santiago, B. X., Drlica-Wagner, A., et al. 2017, *MNRAS*, **468**, 1349
- Pinsonneault, M. H., Elsworth, Y. P., Tayar, J., et al. 2018, *ApJS*, **239**, 32
- Poleski, R., Udalski, A., Gould, A., et al. 2013, *ApJ*, **776**, 76
- Poleski, R., Udalski, A., Gould, A., et al. 2015, in ASP Conf. Ser. 491, Fifty Years of Wide Field Studies in the Southern Hemisphere: Resolved Stellar Populations of the Galactic Bulge and Magellanic Clouds (San Francisco, CA: ASP), 72
- Povich, M. S., Smith, N., Majewski, S. R., et al. 2011, *ApJS*, **194**, 14
- Price-Whelan, A. M., & Bonaca, A. 2018, *ApJL*, **863**, L20
- Price-Whelan, A. M., Hogg, D. W., Rix, H.-W., et al. 2020, *ApJ*, **895**, 2
- Queiroz, A. B. A., Chiappini, C., Perez-Villegas, A., et al. 2020, arXiv:2007.12915
- Ricker, G. R., Winn, J. N., Vanderspek, R., et al. 2015, *JATIS*, **1**, 014003
- Rojas-Arriagada, A., Zasowski, G., Schultheis, M., et al. 2020, *MNRAS*, **499**, 1037
- Roman-Lopes, A., Roman-Zuniga, C. G., Tapia, M., Minniti, D., & Borissova, J. 2020, *ApJS*, **247**, 17
- Sakari, C. M., Shetrone, M. D., Schiavon, R. P., et al. 2016, *ApJ*, **829**, 116
- Schlaufman, K. C., & Casey, A. R. 2014, *ApJ*, **797**, 13
- Schlegel, D. J., Finkbeiner, D. P., & Davis, M. 1998, *ApJ*, **500**, 525
- Schofield, M., Chaplin, W. J., Huber, D., et al. 2019, *ApJS*, **241**, 12
- Schönrich, R., Aumer, M., & Sale, S. E. 2015, *ApJL*, **812**, L21
- Schultheis, M., Zasowski, G., Allende Prieto, C., et al. 2014, *AJ*, **148**, 24
- Scowcroft, V., Freedman, W. L., Madore, B. F., et al. 2011, *ApJ*, **743**, 76
- Scowcroft, V., Seibert, M., Freedman, W. L., et al. 2016, *MNRAS*, **459**, 1170
- Shapley, H. 1938, *Natur*, **142**, 715
- Sharma, S., Stello, D., Bland-Hawthorn, J., et al. 2019, *MNRAS*, **490**, 5335
- Sheffield, A. A., Subrahimovic, A. Z., Refat, M., et al. 2021, *ApJ*, **913**, 39
- Sheinis, A., Anguiano, B., Asplund, M., et al. 2015, *JATIS*, **1**, 035002
- Sheinis, A. I. 2016, *Proc. SPIE*, **9908**, 99081C
- Shipp, N., Drlica-Wagner, A., Balbinot, E., et al. 2018, *ApJ*, **862**, 114
- Skrutskie, M. F., Cutri, R. M., Stiening, R., et al. 2006, *AJ*, **131**, 1163
- Sollima, A. 2020, *MNRAS*, **495**, 2222
- Soszynski, I., Poleski, R., Udalski, A., et al. 2008, *AcA*, **58**, 163
- Stassun, K. G., Oelkers, R. J., Pepper, J., et al. 2018, *AJ*, **156**, 102
- Steinmetz, M., Zwitter, T., Siebert, A., et al. 2006, *AJ*, **132**, 1645
- Stello, D., Zinn, J., Elsworth, Y., et al. 2017, *ApJ*, **835**, 83
- Stutz, A. M. 2018, *MNRAS*, **473**, 4890
- Stutz, A. M., & Gould, A. 2016, *A&A*, **590**, A2
- Stutz, A. M., Gonzalez-Lobos, V. I., & Gould, A. 2018, arXiv:1807.11496
- Taylor, M. B. 2005, in ASP Conf. Ser. 347, Astronomical Data Analysis Software and Systems XIV, ed. P. Shopbell, M. Britton, & R. Ebert (San Francisco, CA: ASP), 29
- Tumlinson, A. 2010, *ApJ*, **708**, 1398
- Udalski, A., Szymanski, M., Kaluzny, J., Kubiak, M., & Mateo, M. 1992, *AcA*, **42**, 253
- Urquhart, J. S., Figura, C. C., Moore, T. J. T., et al. 2014, *MNRAS*, **437**, 1791
- Van der Swaelmen, M., Hill, V., Primas, F., & Cole, A. A. 2013, *A&A*, **560**, A44
- van der Walt, S., Colbert, S. C., & Varoquaux, G. 2011, *CSE*, **13**, 22
- van Leeuwen, F., Le Poole, R. S., Reijns, R. A., Freeman, K. C., & de Zeeuw, P. T. 2000, *A&A*, **360**, 472
- Walker, M. G., Mateo, M., & Olszewski, E. W. 2009, *AJ*, **137**, 3100
- Wenger, M., Ochsenbein, F., Egret, D., et al. 2000, *A&AS*, **143**, 9
- Wilson, J. C., Hearty, F. R., Skrutskie, M. F., et al. 2019, *PASP*, **131**, 055001
- Wittenmyer, R. A., Sharma, S., Stello, D., et al. 2018, *AJ*, **155**, 84
- Wright, E. L., Eisenhardt, P. R. M., Mainzer, A. K., et al. 2010, *AJ*, **140**, 1868
- Xue, X.-X., Ma, Z., Rix, H.-W., et al. 2014, *ApJ*, **784**, 170
- Yan, R., Chen, Y., Lazarz, D., et al. 2019, *ApJ*, **883**, 175
- Zasowski, G., Chojnowski, S. D., Whelan, D. G., et al. 2015a, *ApJ*, **811**, 119
- Zasowski, G., Cohen, R. E., Chojnowski, S. D., et al. 2017, *AJ*, **154**, 198
- Zasowski, G., Johnson, J. A., Frinchaboy, P. M., et al. 2013, *AJ*, **146**, 81
- Zasowski, G., Ménard, B., Bizyaev, D., et al. 2015b, *ApJ*, **798**, 35
- Zinn, J. C., Stello, D., Elsworth, Y., et al. 2020, *ApJS*, **251**, 23
- Zucker, D. B., de Silva, G., Freeman, K., Bland-Hawthorn, J. & Hermes Team 2012, in ASP Conf. Proc. 458, Galactic Archaeology: Near-Field Cosmology and the Formation of the Milky Way, ed. W. Aoki et al. (San Francisco, CA: ASP), 421